Chinese Chemical Letters 37 (2026) 112127

Contents lists available at ScienceDirect

Chinese Chemical Letters

journal homepage: www.elsevier.com/locate/cclet

Micro/nanomotors: From design to biomedicine applications

Xuan Hu[a,1], Ziyan Shen[a,1], Shuang Chao[a,*], Yuxin Pei[a,*], Shoupeng Cao[b,*], Zhichao Pei[a,*]

[a] College of Chemistry & Pharmacy, Northwest A&F University, Yangling 712100, China
[b] College of Polymer Science and Engineering, Sichuan University, Chengdu 610065, China

ARTICLE INFO

Article history:
Received 29 July 2025
Revised 2 November 2025
Accepted 16 November 2025
Available online 18 November 2025

Keywords:
Micro/nanomotors
Propulsion mechanisms
Deep penetration
Biomedical application
Personalized and precision medicine

ABSTRACT

Micro/nanomotors (MNMs) are miniature devices capable of autonomous movement and execution of specific tasks at the micro/nano scale. Compared with traditional drugs, nanomedicines can achieve precise drug delivery through targeting, thereby reducing toxic and side effects on normal tissues. MNMs can utilize inherent fuels in biological systems or absorb external energy and convert it into kinetic energy, which enables them to address the issue that nanomedicines fail to act on the core of lesions due to insufficient tissue penetration. Therefore, they are regarded as excellent candidates for constructing efficient targeted delivery and diagnosis-treatment systems. This review introduces the design and driving strategies of different types of MNMs. Through functionalization of materials and optimization of driving modes, the dual designed objectives of reducing toxic side effects and improving therapeutic efficiency are achieved. In terms of applications, this review mainly introduces the research progress of MNMs in the biomedical field (such as cancer, cardiovascular diseases, wound healing, antibacterial and disease diagnosis-treatment). Finally, the challenges and limitations faced by the practical application of MNMs are discussed, and the future development directions of MNMs are prospected.

© 2026 Published by Elsevier B.V. on behalf of Chinese Chemical Society and Institute of Materia Medica, Chinese Academy of Medical Sciences.

1. Introduction

The emergence of machines and motors has brought convenience to human life [1]. These devices utilize chemical fuels, solar energy, electrical energy, wind energy, and hydropower to obtain power, making tremendous contributions to the spread of human civilization and the improvement of living standards [2,3]. In living organisms, some convert light energy into chemical energy for storage, while natural biological motors such as myosin and kinesin convert chemical energy into mechanical energy, playing a crucial role in intracellular material transport, information transmission, and other biological activities [4,5]. Inspired by this, Feynman *et al.* proposed that micro/nano-scale machines could use external stimuli to actively move and perform specific tasks in their environment [6]. Whitesides and his team invented the first polydimethylsiloxane sheet micro-motor driven by platinum (Pt)-catalyzed hydrogen peroxide (H_2O_2) decomposition, marking the beginning of micro-motor technology [7]. Micro/nanomotors (MNMs) can achieve self-propelled motion using different propulsion mechanisms. According to energy sources, they can be divided into biological propulsion [8], chemical propulsion mediated by enzymes [9,10] and inorganic catalysts [11], and physical propulsion activated by external fields such as light [12,13], ultrasound [14], magnetism [15], and electricity [16].

In the field of biomedical research, compared with traditional nanodrug delivery systems, MNMs possess the ability of autonomous movement, which can enhance drug accumulation at the lesion site, improve targeting, increase drug utilization, and reduce side effects [17,18]. Notably, the simple and efficient design reduces the toxicity and enhance the biocompatibility [19]. Chemically powered MNMs often utilize catalysts or fuels present in the microenvironment of living organisms for energy conversion to drive their autonomous movement. For example, Wan *et al.* developed a nanomotor loaded with L-arginine, which uses nitric oxide synthase (NOS) or reactive oxygen species (ROS) in cells to decompose L-arginine as fuel, generating nitric oxide (NO) that serves both as the driving force for the nanomotor and as a therapeutic agent [20]. Sun *et al.* designed a nanomotor encapsulated with glucose oxidase (GOx) and catalase (CAT), using glucose as fuel to generate oxygen (O_2) through enzymatic cascade reactions to drive the nanomotor, synergistically improving the efficiency of cancer treatment [21]. The use of inherent natural sources in biological systems as fuels ensures better biocompatibility [22,23]. Additionally, MNMs can derive kinetic energy from exogenous sources, enhancing deep tissue penetration of drugs and syner-

* Corresponding authors.
E-mail addresses: chaoshuang@nwafu.edu.cn (S. Chao), peiyx@nwafu.edu.cn (Y. Pei), caoshoupeng@scu.edu.cn (S. Cao), peizc@nwafu.edu.cn (Z. Pei).
[1] These authors contributed equally to this work.

https://doi.org/10.1016/j.cclet.2025.112127
1001-8417/© 2026 Published by Elsevier B.V. on behalf of Chinese Chemical Society and Institute of Materia Medica, Chinese Academy of Medical Sciences.

gizing with respective therapies to improve efficacy [24]. Therefore, based on the application environment of MNMs, leveraging the structural and functional properties of nanodrugs to intelligently design zero-waste, high-efficiency nanomotor delivery systems that respond to specific biological signals or environmental conditions. MNMs address the limitations of traditional nanodrug delivery systems through autonomous movement, flexible regulation, and precise control, demonstrating enormous development potential in the fields of precision medicine, disease diagnosis, and biosensing. This holds significant importance for the advancement of future biomedicine.

Based on this, summarizing and evaluating these important studies in this field will help to better promote research in this direction. This review discusses the latest research progress of MNMs in the fields of biomedicine over the past two years. MNMs are classified according to different propulsion mechanisms, including biological-driven, chemical-driven, physical-driven, and hybrid-driven. It not only introduces the driving mechanisms of MNMs, but also summarizes and analyzes the design and construction strategies of MNMs in different application scenarios, as well as how to achieve precise diagnosis and treatment in the field of biomedicine (such as cancer, cardiovascular diseases, wound healing, antibiosis, disease diagnosis) (Fig. 1). In addition, this review also discusses some considerations and future prospects in the design and application of MNMs.

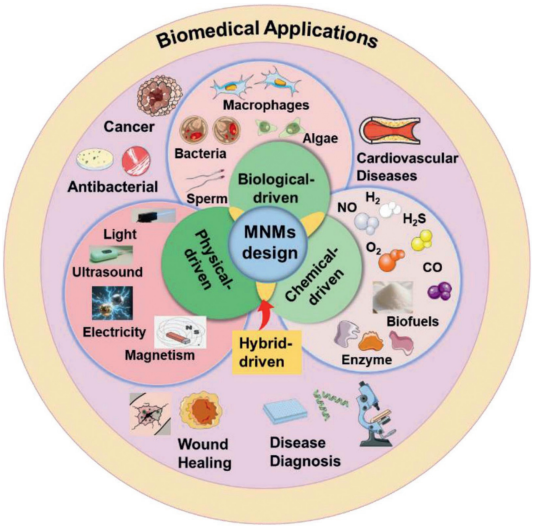


Fig. 1. Schematic diagrams of the design and biomedical applications of MNMs.

2. Different types of MNMs

At present, MNMs can be classified into biological-driven, chemical-driven, physical-driven, and hybrid-driven types according to different propulsion mechanisms (Table 1).

2.1. Biological-driven MNMs

Researchers have found that many natural organisms have the ability to move autonomously in specific environments, such as macrophages, algae, bacteria, and sperm [17]. Biological-driven MNMs combine biological components (including living systems, bioenzymes, and biomembranes) with artificial components to achieve autonomous navigation capabilities and accomplish designated tasks. Based on these movement characteristics, the biological-driven MNMs prepared exhibit excellent biocompatibility and strong adaptability to the complex *in vivo* environment. Furthermore, biological-driven MNMs have the potential to combine micro/nanoparticles with various properties of different organisms, including chemotaxis, magnetotaxis, anaerobism, endowing the developed motors with multiple functions.

Compared with other cells or microorganisms, sperm cells neither express pathogenic proteins nor proliferate to form colonies, also exhibits autokinesia. Thus, sperm micromotors can serve as a biocompatible platform with potential applications in treating cancer and other disease. Xu's group reported a sperm-hybrid micromotor to improve the drug delivery. This system comprises sperm cells responsible for propulsion and drug carrier loaded with dox-

Table 1
Summary of comparisons between different driving approaches.

Types	Propulsion sources	Properties	Advantages	Limitations
Biological-driven	Algae, bacteria, sperm, *etc.*	Bacteria: anaerobic, magnetotactic Algae cells: without pathogenic proteins, self-propulsion Microalgae: efficient propulsion, autofluorescence, phototaxis	Excellent biocompatibility, strong adaptability	Pathogenicity and immunogenicity
Chemical-driven	H_2, O_2, CO_2, NO, H_2S, enzyme, *etc.*	Bubble generation for propulsion or production of asymmetrically distributed products	Gas-driven: enhancement of drug delivery efficiency, combination with gas therapy, and improvement of the pathological environment Enzyme-driven: convenient and continuously generation of biofuels	Enzymes are susceptible to environmental factors, biocompatibility of chemical-driven MNMs, limited by chemical fuels (such as H_2O_2, glucose, or urea)
Physical-driven	Light, ultrasound, magnetism, electricity, *etc.*	Light: the asymmetric structure forms self-thermophoresis Ultrasound: bubble generation for propulsion by sonosensitizers, or asymmetric structures result in uneven distribution of acoustic pressure Magnetism: magnetically driven MNMs target the destination Electricity: asymmetry structure-mediated electrophoretic force	Exogenous energy is environmentally friendly and green, with no risk of depletion Combined with therapies such as phototherapy and ultrasound to improve therapeutic effects	The penetration depth of light irradiation is limited, which imposes limitations on the application of light-driven MNMs
Hybrid-driven	A mixed propulsion source including chemical, biological, physical, and other pathways (encompassing two or three types)	Multiple propulsion mechanisms, such as gas and light-driven, ultrasonic and magnetic-driven	The robustness in complex environments was enhanced and the dependence on fuel resources or other environmental parameters was reduced	Preparation is complex, multi-mode driving requires adjustment and coordination

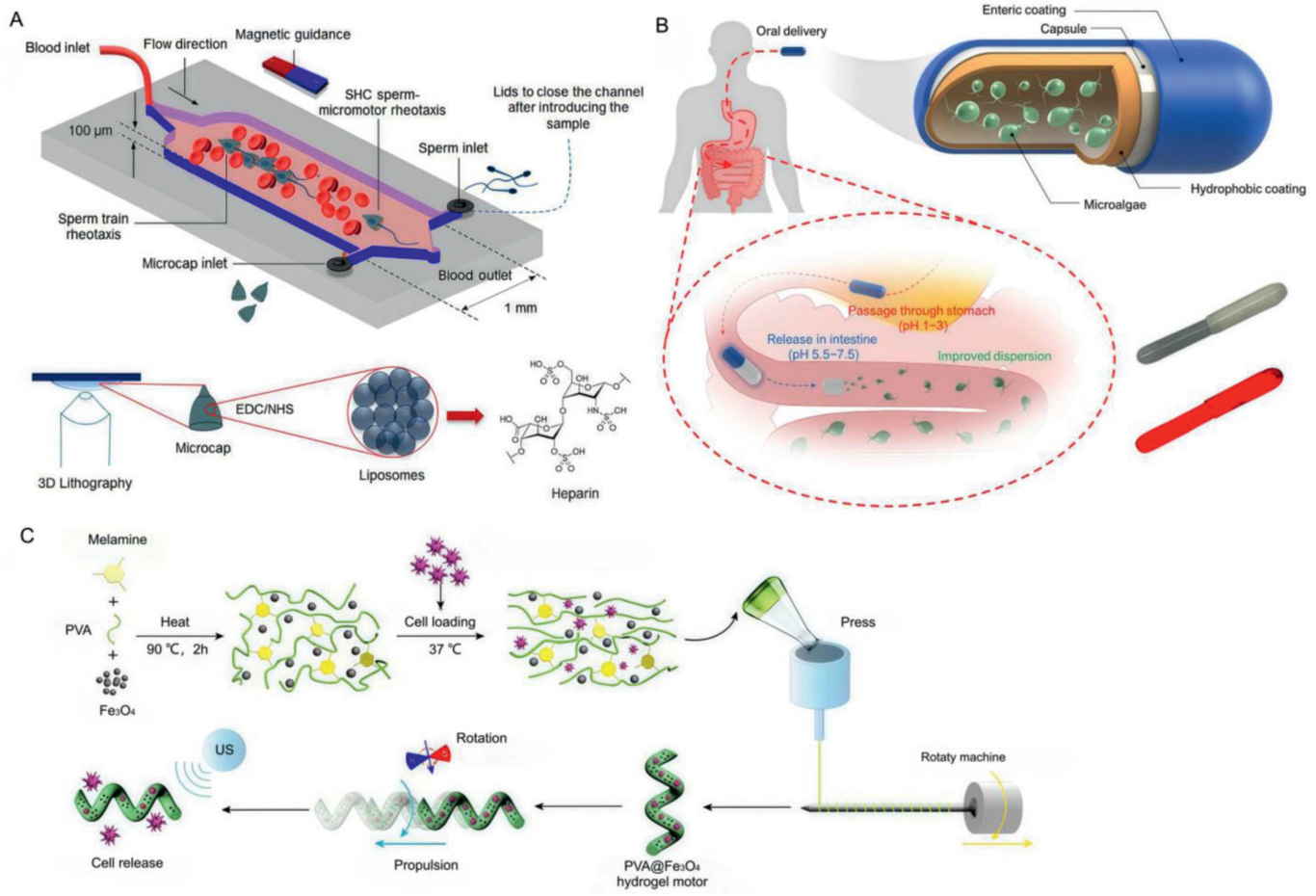


Fig. 2. Schematic diagrams of the biologically-driven MNMs. (A) Schematic diagrams of the preparation of streamlined-horned cap (SHC) hybrid sperm micromotors loaded liposome-heparin and their controllable movement against flowing blood. Reprinted with permission [25]. Copyright 2020, American Chemical Society. (B) Schematic diagrams of algae motors loaded within protective capsules containing an inner hydrophobic coating layer and an outer enteric coating layer, which released after the capsule is degraded in the intestines. Reprinted with permission [26]. Copyright 2022, American Association for the Advancement of Science. (C) Schematic diagrams of the preparation of PVA@Fe_3O_4 hydrogel motor loaded with M1 macrophages. Reprinted with permission [27]. Copyright 2021, Elsevier Ltd.

orubicin (DOX) and a 3D-printed magnetic tubular microstructure. Magnetic forces guide the sperm-hybrid micromotor toward tumor spheroids. Upon impact with the tumor cells, the sperm-hybrid micromotor swim into the tumor and deliver the drug through fusion between the sperm and cancer cell membranes. Sperm cells exhibited efficient and stable drug-loading capacity, self-propulsion, sperm penetration ability, conveniently minimizing toxic side effects and unnecessary drug accumulation in healthy tissues [28]. They also fabricated streamlined hybrid sperm micromotors capable of efficiently and controllably swimming against blood flow (Fig. 2A). By loading liposome-heparin, these micromotors can treat blood clots in the circulatory system [25].

The human body harbors a vast number of microorganisms, whose symbiotic relationship with the human host enables them to play crucial roles in human digestion, nutrition, and immune health. A large number of non-pathogenic bacteria in microorganisms have become important candidates for biologically driven micromotors due to their anaerobic and magnetotactic properties. For example, the facultative anaerobic *Salmonella typhimurium* (*S. typhimurium*) can be used to target tumor tissues by taking advantage of its preference for the hypoxic sites in the tumor core [29]. By coating polydopamine (PDA) molecules onto *S. typhimurium* and leveraging the chemotaxis of *S. typhimurium* toward the hypoxic microenvironment of tumors, the photothermal agent PDA can be delivered to hypoxic tumor tissues. Under light irradiation, it converts light energy into thermal energy to kill tumor cells [30]. Another example of photothermal-driven bacterial motor was prepared by photothermal nanoparticles (NPs) loaded onto *S. typhimurium* and a macrophage membrane-camouflaged, which can stimulate bacteria to accelerate movement under the mild photothermal excitation of near-infrared (NIR) light. This allows the bacterial motor to deeply penetrate tumor tissues and be highly internalized. The photothermal bacterial motor uses the synergistic effect of photothermal effect and bacteria to polarize M2-phenotype tumor-associated macrophages into M1 phenotype, triggering an antitumor immune response and enhancing antitumor efficacy [31].

Also, Luo's team designed two drug delivery methods based on the anaerobic *Bifidobacterium breve* (*B. breve*) and *Clostridium difficile* (*C. difficile*). One is a cargo-carrying method, where gold (Au) nanorods are coupled to *B. breve* for targeting tumors in photothermal ablation; the other is an antibody-directed method, where *C. difficile* spores are first injected into tumor tissues, followed by antibody-conjugated functional NPs for specific targeting of *C. difficile* spores, after which the NPs exert antitumor effects [32]. Nanomotors designed by leveraging the chemotaxis of bacteria toward tumor tissues can improve drug delivery efficiency. Meanwhile, bacteria can serve as an immunogen to enhance antitumor immune efficacy. Additionally, a polymer NP (TDNPP) with aggregation-induced emission (AIE), which was coated on the sur-

face of *Escherichia coli* (*E. coli*) *via* electrostatic interaction. Experimental results showed that TDNPP-*E. coli* invaded and imaged cancer cells more efficiently than free NPs. Under light irradiation, ROS are generated to disrupt bacterial membranes, enabling controlled release of bacterial proteins and enhancing tumor immunity [33]. Magnetotactic bacteria can autonomously propel themselves to the desired position under the guidance of an external magnetic field. For another, Morgan *et al*. designed a biohybrid system of metal-capped Janus NPs adhering to non-pathogenic *E. coli*. When the metal is Fe, bacterial movement can be guided by a magnetic field [34]. With attractive characteristics of bacteria, bacterial-based biohybrid MNMs exhibit excellent biocompatibility and biodegradability, and demonstrating enormous potential in *in vivo* biomedicine.

Microalgae have been used as biologically driven MNMs due to their characteristics such as easy cultivation, efficient propulsion, autofluorescence, and phototaxis. It has great prospects in oral administration to enhance the treatment of gastrointestinal diseases. For example, a capsule system loaded with algal motors for the treatment of gastrointestinal diseases (Fig. 2B). *Chlamydomonas reinhardtii* (*C. pitschmannii*.) swims by synchronously beating its two flagella at a frequency of 50 Hz. Compared with magnesium (Mg) nanomotors relying on chemical energy for movement, algal MNMs do not have the problem of energy depletion. Their movement in the gastrointestinal tract can last for up to 12 h, which makes the distribution of drugs in the gastrointestinal tract more uniform, enhances the residence time of DOX in the gastrointestinal tract, and improves the bioavailability of the drug [26]. In addition, an acidophilic microalga *C. pitschmannii*., which can move in the gastrointestinal tract for a long time. Polymer NPs loaded with green fluorescent dye were used to modify *C. pitschmannii*. By adjusting the surface properties of the NPs, selective targeting of the gastrointestinal tract can be achieved, and the long-term movement in the gastrointestinal tract enables the drug delivery system to be widely distributed throughout the gastrointestinal tract, enhancing drug dispersion and retention [35].

Immunocyte therapy holds enormous potential in the fields of immunomodulation and anti-tumor treatment. However, precisely and efficiently delivering immune cells to the lesion site remains a challenge. To cope with this challenge, a melamine-reinforced polyvinyl alcohol (PVA) hydrogel encapsulating magnetic NPs and macrophages were prepared for cell therapy (Fig. 2C). This system can reach the desired site through magnetic driving, and the hydrogel structure is disrupted by ultrasound to release macrophages for precise treatment. Such macrophage-based biomedical nanomotors provide a new approach for immunocyte therapy and demonstrate great potential in precise cell therapy [27].

Biologically-driven MNMs have witnessed rapid development over the past decade. By leveraging the autonomous motility of biological cells to realize multiple functions, the design of biological-driven MNMs embodies the green and sustainable nature of bionics. However, considering factors such as pathogenicity and immunogenicity, *in vivo* application is confronted with immune system responses and clearance, leaving the development of biologically-driven MNMs still facing significant challenges.

2.2. Chemical-driven MNMs

Chemical-driven MNMs an consume substrates through chemical reactions to generate gases for propulsion or produce asymmetrically distributed products to drive movement *via* gradients in ion concentration. Here, we mainly introduce and summarize the construction strategies of different types of gas-driven motors and enzyme-driven nanomotors.

2.2.1. Gas-driven MNMs

Gas-driven MNMs include those powered by hydrogen (H_2), O_2, carbon dioxide (CO_2), NO, hydrogen sulfide (H_2S), *etc.* (Table 2) [36–42]. MNMs utilize endogenous fuels or fuels carried by themselves to undergo chemical reactions, generating bubbles to achieve autonomous movement.

For instance, a dandelion-shaped nanomotor was constructed, which composed of Au nanorods and titanium dioxide NPs. This Janus nanomotor exhibits significantly enhanced NIR-catalyzed H_2 evolution performance. H_2 generated at one end of Au NRs serves as an effective driving force to propel the nanomotor forward, promoting cell uptake and improving the accumulation and distribution of tumors. In the presence of NIR light, the content of nanomotors accumulated in tumor sites is approximately 1.8 times higher than that without NIR irradiation, and the nanomotors are more uniformly distributed in tumors, providing a new approach for efficient radiotherapy [43].

Another example of H_2-driven nanomotor is asymmetrically sputtering gallium (Ga) onto zinc (Zn) NPs, a Janus Ga-Zn micromotor with good biocompatibility and biodegradability in simulated gastric acid was constructed. Zn reacts with acid to generate H_2 and the bubbles push the movement. Meanwhile, this movement is enhanced by the galvanic effect of Ga-Zn. The generated Ga^{3+} cations from micromotor degradation can kill *Helicobacter pylori* in the stomach. Additionally, modifying Fe_3O_4 NPs on Ga/Zn micromotors may help achieve controlled navigation, enabling the micromotors to remain at the infection site for a long time and enhance therapeutic efficiency [36]. Similarly, self-propelled Janus Ga/Mg bimetallic micromotors with good biocompatibility and antibacterial properties have also been reported. H_2 bubbles generated by the Mg-water reaction enable the micromotors to break through the biological barriers of saliva and gingival crevicular fluid, entering the bottom of periodontal pockets. Antibacterial ions Ga^{3+} eliminate deep *Porphyromonas gingivalis*. This micromotor has shown strong antibacterial and anti-inflammatory activities in both *in vitro* and *in vivo* studies [44].

The typical characteristics of the tumor microenvironment (TME), including hypoxia, weak acidity, and high H_2O_2 content, make the design of O_2-driven MNMs that can not only drive nanomotors but also consume H_2O_2 in tumor tissues, alleviate hypoxia, and improve the TME. For instance, researchers designed a core-shell structured metal-organic framework (MOF) with indocyanine green (ICG, a photosensitizer) and chemotherapy drug DOX encapsulated in Materials of Institute Lavoisier-88 (MIL-88) as the core and zeolitic imidazolate framework 8 (ZIF-8) as the shell. The iron ions in MIL-88 induce a Fenton-like reaction with

Table 2
Summary of different gas-driven MNMs.

Substrate	Driving sources	Size	Speed (μm/s)	Application field	Ref.
Janus Ga/Zn micromotors	H_2 bubbles and Ga-Zn galvanic effect	~8.9 ± 0.7 μm	383	Bacterial infections	[36]
Au@Pt NPs on liposomes	O_2 driven	~100 nm	44.95 ± 4.1	Biomedicine and plant nanotechnology	[37]
Pt-MOFs nanomotors	O_2 driven	79–297 nm	3.8	Surgical wound healing	[35]
AuNRs with SiO_2 nanomotors	CO driven	120 ± 12.8 nm	25.968	Bladder cancer diagnosis	[39]
PMPC/A nanomotors	NO driven	~206 nm	4.12	Spinal cord injury	[40]
LPDA@IIA-Shp	NO driven	~92.8 nm	–	Ischaemic stroke	[41]
PCM@siRNA nanomotors	H_2S driven	50–100 nm	3.5	Parkinson's disease	[42]

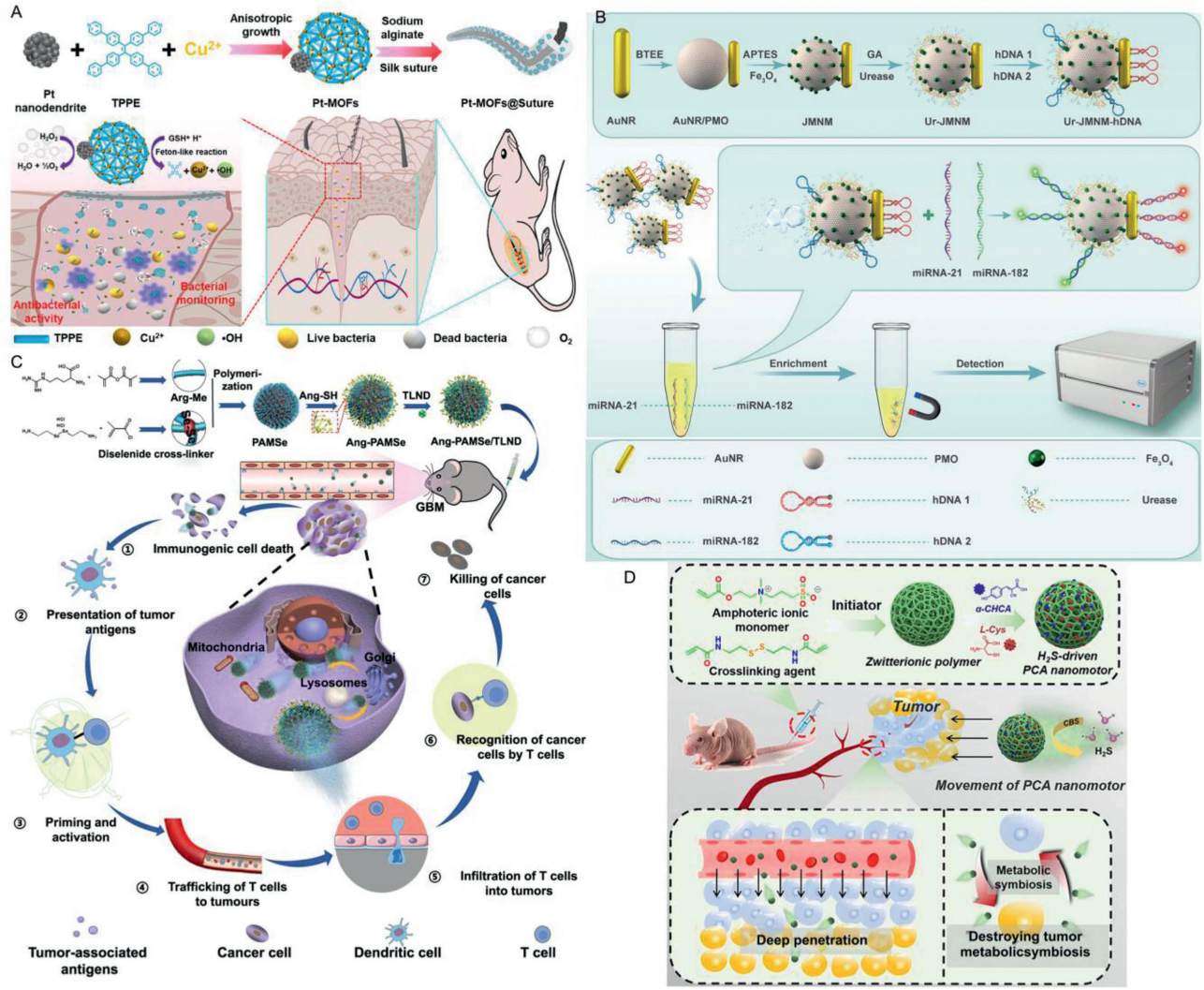


Fig. 3. Schematic diagrams of the gas-driven MNMs. (A) Schematic illustration of the formation and application of O_2-driven nanomotors (Pt-MOFs) infected by microenvironment for bacterial monitoring and antibacterial activity. Reprinted with permission [38]. Copyright 2025, Wiley-VCH. (B) Schematic diagrams of the synthesis process of CO_2-driven nanomotors (Ur-JMNM-hDNA) and detection for miRNA biomarkers (miRNA-21 and miRNA-182) in urine samples for bladder cancer screening. Reprinted with permission [39]. Copyright 2025, American Chemical Society. (C) Schematic diagrams of the design of NO-driven nanomotors and proposed mechanism of enhancing immunotherapy for GBM. Reprinted with permission [51]. Copyright 2023, Springer Nature. (D) Schematic diagrams of the design of H_2S-driven nanomotor for tumor metabolism symbiosis. Reprinted with permission [52]. Copyright 2021, Wiley-VCH.

excessive H_2O_2 in the TME to generate O_2, enhancing the efficacy of photodynamic therapy (PDT) [45]. Also, Au@Pt NPs also have been reported exhibit highly similar CAT activity. The fluidity of the liposomes causes the Au@Pt adsorbed on the liposomes to spontaneously aggregate, forming an asymmetric distribution. This nanomotor can respond to exogenous and endogenous H_2O_2 to generate O_2, directionally propel the nanomotor, and show good biocompatibility [37]. Additionally, Liang *et al.* prepared medical sutures coated with Janus-type nanomotors (Pt-MOF). The Pt-MOF nanomotors are constructed by selectively anisotropic growth of copper-based tetra(4-pyridylphenyl)ethylene (TPPE) nanoscale MOFs on Pt NPs (Fig. 3A). By catalyzing H_2O_2 to generate O_2 bubbles, they exhibit efficient self-propulsion, enhance penetration and diffusion in biofilms, and dissociated Cu^{2+} produces hydroxyl radicals (•OH) through the Fenton reaction. Meanwhile, protonated TPPE aggregates are generated on the bacterial surface, leading to fluorescence. Pt-MOF can serve as both an antibacterial agent for treating bacterial infections and an imaging tool for monitoring surgical sites [38]. Zhang *et al.* designed an inhalable bionic nanomotor (MHLP) for treating pulmonary thrombosis, which can mimic platelet functions to cross the pulmonary mucosal barrier and target pulmonary thrombi. MHLP responds to the thrombus microenvironment by using ROS as fuel to generate O_2 and NO, promoting the release of loaded anticoagulant drugs. These gases can also regulate the thrombus-inflammatory microenvironment, promoting the polarization of macrophages from a pro-inflammatory to an anti-inflammatory phenotype and downregulating the expression levels of inflammatory factors. MHLP features low cost, flexible synthesis, and high catalytic activity. Compared with NIR light-driven nanomotors limited by light penetration depth and ultrasound-driven nanomotors restricted by the special alveolar structure of lung tissue, MHLP uses H_2O_2 as a chemical fuel for self-driven nanomotor therapy of pulmonary thrombosis, which well embodies the efficient utilization of resources and zero waste [46].

Urea is abundant in the bladder and can be decomposed into CO_2 and ammonia (NH_3). Therefore, the design of CO_2-driven micro-nanomotors holds potential for the treatment of bladder diseases. Polymer nanomotors containing urease (Ure) move around in the bladder by converting urea into CO_2 and NH_3, and they can remain in the bladder for a long time after multiple urinations, showing good biocompatibility and bioavailability [47]. To specif-

ically detect bladder cancer biomarkers miRNA-21 and miRNA-182, a nanomotor with a Au nanorod-mesoporous silica Janus structure was prepared as a recognition probe for target miRNAs (Fig. 3B). By attaching Fe_3O_4 and Ure to the SiO_2 surface, hDNA was designed as a biorecognition element and immobilized on Fe_3O_4 and Au NPs as a recognition probe for target miRNAs. In urea solution, Ure catalyzes the conversion of urea into NH_3 and CO_2, driving the nanomotor for up to 60 min. This nanomotor probe can effectively detect miRNAs in spiked urine samples, with quantitative detection limits of 29 and 362 fmol/L for miRNA-21 and miRNA-182, respectively, providing a novel non-invasive strategy for bladder cancer detection [39]. Furthermore, Au nanorods encapsulated in human serum protein NPs, loaded with Ure and ICG, and surface-modified with folate receptors enable the nanomotors to target tumor cells. In the presence of urea and light, Ure decomposes urea to generate CO_2, driving the movement of nanomotors and enhancing drug uptake by cancer cells. More importantly, the photothermal conversion capability of nanomotors to NIR light not only enhances the catalytic activity of Ure but also improves its movement in the presence of urea. Compared with traditional Ure-driven nanomotors, this nanomotor improves cell uptake at tumor sites and exhibits better phototherapeutic anticancer effects [48].

NO is a well-known gaseous signaling molecule with multiple biological functions, holding great potential in the field of disease treatment [49,50]. Wan *et al*. first reported a NO-driven nanomotor, which uses medical fluorescent hyperbranched polyamide (HPAM) and biocompatible zwitterionic L-arginine to synthesize hyperbranched polyamide/L-arginine (HLA) nanomotors. These nanomotors exhibit excellent motility *in vitro*, and both the reactants and products can have beneficial effects on the human body, truly achieving zero-waste and self-destructing nanomotor [20].

Subsequently, the same research group designed and synthesized another NO-driven zwitterionic polymer nanomotor, loaded with the chemotherapeutic drug Lonidamine and modified with angiopep-2 peptide, which can specifically target glioblastoma (GBM) (Fig. 3C). The guanidine groups in the nanomotor react with the highly expressed ROS and inducible NOS in the GBM microenvironment to generate NO. Additionally, the nanomotors exhibit chemotaxis in response to the ROS/iNOS concentration gradient in the GBM microenvironment to achieve targeting [51]. Nanomotors based on poly(2-methacryloyloxyethyl phosphorylcholine) (PMPC)/L-arginine (PMPC/A), which are driven by NO release and show chemotaxis toward higher ROS regions (nerve injury sites), thus promoting cell growth at the injury site [41]. Since atherosclerosis is characterized by high concentrations of ROS and upregulated inflammatory markers at the lesion site, NO-driven nanomotors exhibit chemotaxis toward the lesion site. In this process, the released NO, besides serving as a driving force, increases the probability of contact between NPs and target cells, and also has beneficial effects on the proliferation and migration of endothelial cells, improving the microenvironment at the lesion site [53]. Also, a stroke-homing peptide-modified L-arginine-doped mesoporous PDA nanodrug delivery system loaded with tanshinone IIA (IIA). It uses the abundant ROS in the stroke area as fuel to generate NO and achieve deeper penetration of the nanodrug delivery system. The multifunctional enzymatic activity of PDA and the potent anti-inflammatory properties of IIA work synergistically to enhance the treatment of ischemic stroke [42].

The H_2S molecule plays an important role in human physiological activities. Studies have shown that exogenous H_2S can promote cellular glucose uptake and inhibit proton efflux [54]. Wan *et al*. designed an H_2S-driven nanomotor, selecting the zwitterionic sulfobetaine methacrylate as the polymerization monomer, *N*,*N*′-bis(acryloyl) cystamine as the crosslinker, and loading L-cysteine (L-Cys) and the proton pump inhibitor α-CHCA (Fig. 3D). L-Cys is catalyzed by cystathionine β-synthase *in vivo* to generate H_2S gas and L–serine. H_2S can promote tumor cells to uptake glucose during the movement of NPs, leading to the production of a large amount of lactic acid, inhibiting the efflux of intracellular protons, and causing acidosis in tumor cells. Meanwhile, α-CHCA can inhibit the expression of monocarboxylate transporter 1/4 (MCT-1/4), disrupt the lactic acid transfer chain between tumor cells, lead to excessive intracellular accumulation of lactic acid, thereby aggravating the acidosis process, and finally destroy the metabolic symbiosis of tumor cells to induce tumor cell apoptosis [52]. Another example is that NPs were prepared through free radical polymerization of L-Cys derivatives modified by polyethylene glycol and 2-methacryloyloxyethyl phosphorylcholine (MPC). Due to the special structure of MPC, which is similar to acetylcholine, it can interact with acetylcholine receptors on the surface of cerebrovascular endothelial cells to penetrate the blood-brain barrier (BBB). In addition, the specific affinity of neuronal 3-mercaptopyruvate sulfurtransferase for L-Cys ensures that the H_2S nanomotor is rarely released in normal tissues and shows chemotaxis to neuronal cells. The H_2S nanomotor has good biocompatibility, which can reduce neuronal damage and promote nerve growth [55]. Similarly, an amphoteric ion-based H_2S donor nanomotor was reported that can encapsulate siRNA, protect its activity, and effectively penetrate the BBB to achieve efficient siRNA delivery, representing the first use of nanomotors for siRNA delivery in the treatment of Parkinson's disease [43]. Furthermore, dual gases of NO and H_2S driven nanomotor were constructed for cardiovascular disease. NO and H_2S synergistically regulate the microenvironment of myocardial infarction with ischemia-reperfusion injury, reduce the inflammatory level, and promote recombinant granulocyte colony-stimulating factor (G-CSF) to exert cardioprotective effects [56].

Gas-driven nanomotors can not only propel the drug delivery system of MNMs by generating bubbles to address the obstacle of drug delivery. but also consume endogenous fuels to produce gas, thereby "turning waste into treasure". This process improves the microenvironment at the treatment site, and the gas therapy can synergize with drugs to enhance the therapeutic effect. This embodies the "one stone, three birds" effect in the construction strategy of MNMs.

2.2.2. Enzyme-driven MNMs

Enzymes are naturally occurring biological catalysts and exhibit better biocompatibility compared with inorganic catalysts. As there are numerous enzymes and substrates in the body, organisms can continuously generate biofuels, enabling long-term propulsion of nanomotors. Therefore, developing enzyme-driven nanomotors is highly convenient. Enzyme-driven MNMs show great development prospects in the fields of disease treatment (Table 3) [57–64]. The movement mechanisms of enzyme-driven nanomotors include bubble propulsion, self-diffusiophoresis, and self-thermophoresis, among others [65].

In recent years, many reported MNMs use H_2O_2 as fuel because it can decompose into water (H_2O) and O_2, which is harmless to organisms and the environment, making it a "green fuel". The O_2 bubbles propel the motor movement, and CAT, a common catalyst for decomposing H_2O_2, has been widely studied and reported due to its good biocompatibility. A hyaluronic acid-modified silica Janus nanomotor loaded with CAT, which not only reduces bacterial infection by decomposing H_2O_2 but also converts H_2O_2 into O_2 to endow it with active movement ability, promoting its extensive diffusion at the lesion site. Tumor tissues contain more H_2O_2 than normal tissues because the rapid proliferation of tumor cells requires high concentrations of ROS [66]. Therefore, using this difference in H_2O_2 concentration gradient helps design chemotactic nanomotors to achieve targeted drug delivery. For instance, a cascade enzyme-powered nanomotor using CAT and GOx as catalysts to consume glucose at the tumor site, generate O_2 bubbles to drive

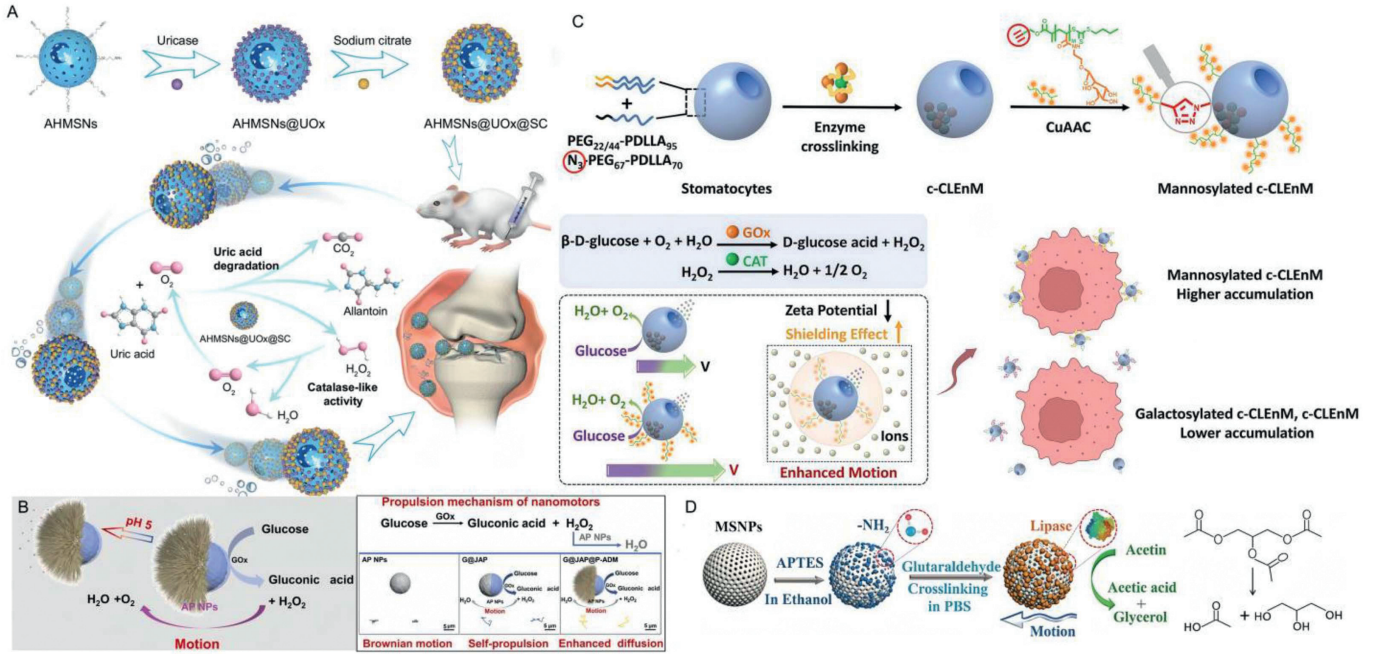


Fig. 4. Schematic diagrams of the enzyme-driven MNMs. (A) Schematic illustration of the fabrication of AHMSNs@UOx@SC nanomotor and the mechanism of nanomotor for gout therapy. Reprinted with permission [58]. Copyright 2025, Springer Nature. (B) Schematic diagrams of the PMETAC brushes and GOx functionalization of glucose-powered Janus nanomotors for enhancing the drug dosage and delivery efficiency. Reprinted with permission [60]. Copyright 2024, Elsevier Ltd. (C) Schematic diagrams of mannosylated compartmentalized cross-linked enzymatic nanomotors (Man-c-CLEnM), which led to a synergistic effect by improving both motility in a physiological environment and enabling targeting capability toward cancer cells. Reprinted with permission [70]. Copyright 2025, Wiley-VCH. (D) Schematic diagrams of the functionalization strategy for the preparation of the lipase-based nanomotors, whose motion is triggered by the catalytic reaction with triacetin. Reprinted with permission [71]. Copyright 2019, Wiley-VCH.

the motor, and simultaneously alleviate hypoxia at the tumor site, making tumor cells sensitive to glucose levels and exerting a synergistic enhanced antitumor effect through starvation therapy [57]. Also, a MNMs with CAT-encapsulated MOF NPs attached to bacterial cellulose nanocapsules, where enzyme-mediated O_2 bubble generation provides propulsion in the presence of H_2O_2 [67].

Urea is also an important nitrogen-containing metabolite in the human body. In recent years, urea has become a commonly used fuel for the movement of MNMs, which can be hydrolyzed by Ure into NH_3 and CO_2 [66]. An enzymatic hollow mesoporous nanomotor was fabricated for efficient treatment of gout (Fig. 4A). By preparing amine-functionalized hollow mesoporous silica NPs (AHMSNs), loading uricase (UOx) and sodium citrate (SC), a self-cascade catalytic system (AHMSNs@UOx@SC) was formed. UOx degrades uric acid into allantoin and H_2O_2, and SC catalyzes the conversion of H_2O_2 into O_2 and H_2O. O_2 further enhances the catalytic hydrolysis of uric acid and drives the movement of nanomotors, enhancing the diffusion ability of AHMSNs@UOx@SC, thus producing more efficient gout treatment activity [58]. Additionally, Ure encapsulated in ZIF-8 to obtain ZIF-8@Ure (ZU-I) nanomotors. ZU-I exhibits strong diffusivity in the presence of urea, and still shows strong motility under conditions of high temperature, proteases, and organic solvents. Compared with traditional enzyme nanomotors with enzymes modified on the outside, it shows stronger penetrability in small intestinal mucus containing proteases. This work provides a new strategy for optimizing the performance of enzyme nanomotors and protecting enzyme activity [68]. Also, Ure-driven nanomotor loaded with a stimulator of interferon genes (STING) agonist, which can effectively activate immune cells in the bladder wall. By intravesical instillation, the nanomotors can effectively penetrate and retain in the bladder. In a mouse bladder cancer model, the nanomotors containing STING agonist showed good antitumor efficacy. Ure-driven nanomotors will provide a new approach for the immunotherapy of bladder cancer [59]. Moreover, Hortelao *et al.* constructed mesoporous silica NPs and Au NPs containing Ure as nanomotors and performed radioactive labeling. After intravesical injection of the nanomotors into the bladders of mice, when urea was injected, the nanomotors were still evenly distributed, while the non-motile nanomotor (without Ure and urea) group showed continuous phase separation, indicating that the self-propelled movement of nanomotors promotes convection and mixing in biological reservoirs [69]. Based on the microenvironment rich in endogenous urea, Ure-driven MNMs have been designed. The MNMs exhibit excellent biocompatibility, reduce toxi-

Table 3
Summary of different enzyme-driven MNMs.

Substrate	Enzyme	Size (nm)	Speed (μm/s)	Application field	Ref.
CAuNCs@HA-HK-2 siRNA	CAT	171.53 ± 1.40	25.25 ± 0.33	Triple negative breast cancer	[57]
AHMSNs@UOx@SC	UOx	279	7.19 ± 0.70	Gout	[58]
STING@nanomotor	Ure	600	–	Bladder cancer	[59]
G@JAP@P-ADM	GOx	92	5.7	Drug delivery for tumor	[60]
Lipase-AMSN-S	Lipase	250–330	~8	Design of intestinal mucus-penetrating nanomotors for drug delivery	[61]
Fe_3O_4@SiO_2-Laccase	Laccase	590.4	–	Removal of multiple pollutants	[62]
PDLR	LOX	~120	–	Tumor radiotherapy enhancement	[63]
MF-NPs	Collagenase	~500	~22	Development of medical nanoformulations	[64]

city and side effects on normal tissues, and enhance therapeutic efficacy.

Glucose is abundant in biological environments and serves as the primary energy source for organisms. GOx can decompose glucose into gluconic acid and H_2O_2, and it can combine with enzymes such as Ure and CAT. Harnessing the inherent energy within organisms to design and develop enzyme-driven reaction nanomotors offers better biocompatibility and considerable development potential. GOx and poly[2-(methacryloyloxy)ethyltrimethylammonium chloride] (PMETAC) polymer form a Janus structure on one side of Au-Pt NPs, with drugs adsorbed onto PMETAC chains to create the pH-responsive glucose-driven Janus nanomotor (G@JAP@P-ADM) (Fig. 4B). In glucose solution, the cascade reaction of G@JAP@P-ADM provides self-propulsion, enhanced diffusion, and absorption capabilities to accelerate movement toward tumor tissues. Upon reaching tumor cells, drugs are released from PMETAC chains *via* pH-responsive mechanisms in the mildly acidic microenvironment, improving drug delivery efficiency [60]. Similarly, A chemical/magnetic hybrid micromotor was designed, which composed of GOx and magnetite (Fe_3O_4) magnetic NPs modified cubic calcium carbonate ($CaCO_3$) microparticles (CCMPs). In the presence of glucose, the nanomotor exhibits glucose concentration-dependent self-propulsion and can be guided to target cancer cells by an external magnetic field to enhance cellular uptake. The GOx-initiated biocatalytic reaction depletes intracellular glucose, further reducing cancer cell viability and significantly improving anticancer efficacy [72]. Also, Liu *et al.* constructed mannosylated nanomotors encapsulated with GOx and CAT, which can drive the autonomous movement of the motors in the presence of glucose (Fig. 4C). The modification with glycopolymers not only endows the nanomotors with targeting ability to cancer cells, but also improves their motility in the physiological environment, synergistically accelerating the movement of the motors and expanding their potential applications in nanomedicine [70].

Lipids are key components of gastrointestinal mucus, and pancreatic lipase is a hydrolase that can catalyze the decomposition of lipids such as glycerides in the intestine into fatty acids and glycerol. Lipase-driven nanomotors have been reported (Fig. 4D). Lipase stochastic modified on mesoporous silica NPs, which can swim in triglyceride solution, improving the degradation efficiency of triglyceride substrates. Lipase can also act as a highly efficient cleaner to remove the triglyceride droplets, making it suitable for biological and environmental applications [71]. Similarly, Ban's research group designed mesoporous silica nanomotors with asymmetric structures and modified the surface with lipase to prepare functional nanomotors. After intestinal injection, the lipase-driven nanomotors showed deeper mucus penetration and higher transepithelial transport than the nanosized particles without lipase modification. This study provides valuable insights for the design of nanomotors that can penetrate intestinal mucus for drug delivery [61].

Laccase (E.C. 1.10.3.2), a multicopper oxidase, can catalyze various phenolic pollutants and serves as an environmentally friendly substance for environmental remediation [73]. Laccase-driven magnetic silica nanomotors were prepared, which efficiently degrade multiple pollutants in solutions of bisphenol A (BPA, a phenolic pollutant), Congo red (CR, a carcinogenic azo dye), and their mixtures. Laccase nanomotors exhibit higher efficiency and recyclability in removing various pollutants from waste water [62].

Due to the rapid proliferation, tumor cells need to consume a large amount of energy. Because of the hypoxia in tumor tissues, anaerobic glycolysis consumes glucose to produce a large amount of lactic acid. High levels of lactic acid are a hallmark of the TME, and the deeper into the tumor, the more lactic acid content [74]. Therefore, a lactate oxidase (LOX)-driven multifunctional nanoradiosensitizer (PDLR) was designed. Multifunctional Pt NPs with CAT-like activity as the delivery carrier, loaded DOX and LOX through electrostatic adsorption, and coated the outer layer with a cRGD-modified liposome membrane. *In vitro* and *in vivo* studies have shown that PDLR exhibits the best deep penetration ability in tumor sites with high lactic acid levels, can improve the hypoxic environment of tumor tissues, and enhance the antitumor efficacy [63].

Collagen is a major component of the extracellular matrix (ECM), and collagenase can decompose collagen. Therefore, designing collagenase-driven nanomotors can enhance deep drug delivery. Chen and collaborators have reported CAT- and collagenase-dual-functionalized zeolitic imidazolate framework-90 (ZIF-90) nanomotors, which demonstrated enhanced tissue penetration in 3D tumor spheroids and improved drug delivery efficiency in solid tumors [75]. Additionally, a collagenase-driven superparamagnetic NPs were designed. Under a Ga ion gradient, the swimmers in collagen gels exhibit rapid and directional movement. Meanwhile, under an alternating magnetic field, the paramagnetic NPs generate heat to damage cells. The collagenase nanomotor enhances the tissue penetration of the nanodrug delivery system to achieve efficient drug delivery [64].

Enzyme-driven MNMs show great development prospects in the fields of disease treatment, especially those enzymes more related to specific diseases and more selective for pathological environments. MNMs developed using disease-related enzymes or substrates may have greater potential for targeted diagnosis and treatment. However, since the activity of enzymes is susceptible to environmental factors such as temperature and pH, there is a high risk of inactivation before reaching the treatment site. In addition, for MNMs driven by chemical fuels, it is necessary to consider whether adding fuel to the system will alter the microenvironment, whether the fuel concentration can drive the movement of nanomotors, or whether the products generated by catalytic reactions will cause toxic reactions in our bodies. Therefore, it is still necessary to develop more efficient, stable, and biocompatible nanocarriers, and to find a "green fuel" to significantly improve the overall performance of chemical nanomotors and fully unleash their potential.

2.3. Physical-driven MNMs

Compared with chemical-powered MNMs, physical MNMs by external fields such as light, ultrasound, magnetism, and electric fields, are not limited by chemical fuels (such as H_2O_2, glucose, or urea) [76]. In addition, external field energy can not only provide driving force for motor movement but also be combined with therapies such as phototherapy and ultrasound to improve therapeutic effects (Table 4) [77–84].

2.3.1. Light

Light-driven nanomotors require two key components: photothermal materials and asymmetric structures. Photothermal materials convert light energy into heat energy, and the asymmetric heat distribution caused by the asymmetric structure forms self-thermophoresis, which propels the movement of nanomotors.

As a green, clean and environmentally friendly energy source, light energy features spatiotemporal selectivity and minimal invasiveness. The design of light-driven nanomotors can not only enhance the ability of drug delivery systems to penetrate deep into tissues, but also synergize with photothermal therapy (PTT) and PDT to improve therapeutic efficacy. For instance, Feng *et al.* designed a core-shell nanomotor PPy@COF-Por with polypyrrole (PPy) as the core and porphyrin-decorated covalent organic frameworks (COFs) as the shell. The PPy core acts as an efficient photothermal agent under 808 nm light, exhibiting excellent pho-

Table 4
Summary of physical-driven MNMs.

Substrate	Propulsion sources	Size (nm)	Speed (μm/s)	Contributions	Application field	Ref.
PPy@COF-Por	808 nm NIR light	227.84 ± 14.19	14.82	The high infrared thermal imaging/PA imaging/fluorescence trimodal imaging-guided combined PTT/PDT	HCT116 tumor	[77]
AuNR/PMO@CPG	808 nm NIR light	190	26.3	Boosting of PTTy-induced ICD in tumor immunotherapy	Cancer photoimmunotherapy	[78]
AHNMs-DOX	1064 nm NIR-II light	284 ± 11.0	~50	First Developmment of a powerful NIR-II light-driven nanomotor and its successful application in enhanced immunochemotherapy	Enhancement of cancer immunochemotheray	[79]
BMO-QCS-HA	Ultrasound and NO bubbles	~248	6.89	Introduction of a new paradigm for ultrasound-actuated nanomotors and a unique strategy for reprogramming TAMs to enhance cancer immunotherapy	Enhance cancer immunotherapy	[80]
MMSNP	Acoustic-magnetic responsive	~500	7.2 ± 0.1	Innovative integration of magnetic targeting spatial localization and ultrasound-driven directional penetration	Orally administered drug delivery for gastrointestinal diseases	[81]
ABP-MNs	Rotating magnetic field	23.2 ± 2.3	–	Providing an effective mechano-based therapy in treating solid tumors	Treatment of solid tumors	[82]
MMSNBs	Magnetic field and CAT-powered	~270	7.59	The direction can be controlled under effective magnetic field, and it can be recycled through the magnetic field for reutilization	Detecting and removing heavy metal ions	[83]
hBT-CuS@PDA	Light and pyroelectric materials	~248	–	Self-protrusion, PEDT and PTT effects and nanozyme catalysis were integrated to demonstrate their synergistic effect	Antitumor	[84]

tothermal conversion to enable directional movement. The porphyrin component serves as a photosensitizer, generating singlet oxygen ($^1O_2$) under 660 nm laser irradiation for potent PDT. This novel NIR driven COF nanomotor integrates PTT and PDT, demonstrating robust antitumor effects against human colorectal carcinoma cells in both *in vitro* and *in vivo* models [77]. Similarly, Zhang and co-workers synthesized a walnut-shaped PDA nanomotor (PDA-PEG) modified with methoxypolyethylene glycol amine (mPEG-NH_2), driven by NIR light. Loaded with photosensitizer ICG *via* electrostatic/hydrophobic interactions and chelated with Fe^{3+}, PDA-PEG's asymmetric morphology under NIR light creates uneven photothermal effects and thermal gradients for autonomous movement. Fe^{3+} catalyzes endogenous H_2O_2 to generate O_2, relieving tumor hypoxia and enhancing $^1O_2$ production for tumor cell killing. *In vivo* experiments confirm its synergistic PTT/PDT efficacy [85]. Xing's group designed single-atom copper-coordinated nitrogen-doped jellyfish-like mesoporous carbon nanomotors (Cu-JMCNs), where copper single atoms catalyze H_2O_2 into toxic $^{\bullet}OH$ for chemodynamic therapy (CDT). NIR light triggers self-thermophoresis *via* the jellyfish-like asymmetric structure and photothermal properties of carbon. *In vivo* studies show that combining single-atom copper for CDT with NIR propulsion achieves >85 % tumor inhibition [86].

Nano-based photoimmunotherapy has emerged as an attractive strategy for eliminating tumors and activating host immune responses. However, therapeutic efficacy is severely constrained by low tumor penetrability and the immunosuppressive TME [87]. Designing light-driven nanomotors can address these challenges by enabling deep tumor penetration, photothermal ablation, and light-triggered immunotherapy. For example, Zhang *et al.* designed an asymmetric NIR-driven nanomotor constructed from Au nanorods and mesoporous organosilica nanospheres (PMOs), loaded with the immunoadjuvant CPG ODN. Under NIR irradiation, the nanomotor exhibits excellent PTT, generating active movement at 19.3 μm/s for deep tumor penetration and accumulation *in vivo* (Fig. 5A). Additionally, photothermal ablation triggers immunogenic cell death (ICD), producing *in-situ* tumor vaccines that synergize with CPG to inhibit tumor growth [78]. Also, Wang *et al.* developed a near-infrared II (NIR-II) light-driven hydrogel nanomotor encapsulating DOX. During microfluidic fabrication, hydrogel droplets containing Fe_3O_4@Cu_9S_8 NPs (with DOX loaded) are magnetically aggregated on one side, then solidified by UV light. Under NIR-II irradiation, Cu_9S_8 converts light energy to heat, creating internal thermal gradients due to its asymmetric distribution, which drives self-thermophoresis. This significantly accelerates movement and promotes deep tumor penetration. DOX induces ICD to activate immunity, effectively enhancing cancer immunochemotherapy [79].

Light-driven nanomotors combined with PDT also show great application prospects in anti-biofilm and antibacterial fields [89]. Deng *et al.* fabricated a novel NIR-driven CSIL nanomotor by co-loading ICG and lysostaphin (Ly) onto spiky yolk-shell structured C/SiO_2@C NPs (Fig. 5B). This nanomotor inhibits bacterial growth, promotes the polarization of macrophages from M1 to M2 during wound healing, and eradicates MRSA biofilms and heals wounds through a cascade PDT strategy [88]. Liu and co-workers reported the preparation of NIR-II light-driven dual-plasmonic (AuNR-SiO_2–Cu_7S_4) antibacterial nanomotors with the expected Janus configuration by overgrowing copper-rich Cu_7S_4 nanocrystals on Au nanorods. These nanomotors can be used for photoacoustic (PA) imaging, exhibit excellent photothermal properties, and synergize with photocatalysis to treat bacterial infections. The motile behavior of the nanomotors promotes transdermal penetration and enhances the interaction between substances and bacteria. More importantly, the directional navigation and synergistic antibacterial activity of the nanomotors can be synchronously driven by NIR-II light. The combination of active movement and enhanced antibacterial activity has achieved the expected good antibacterial effect in a mouse model of abscess infection [90].

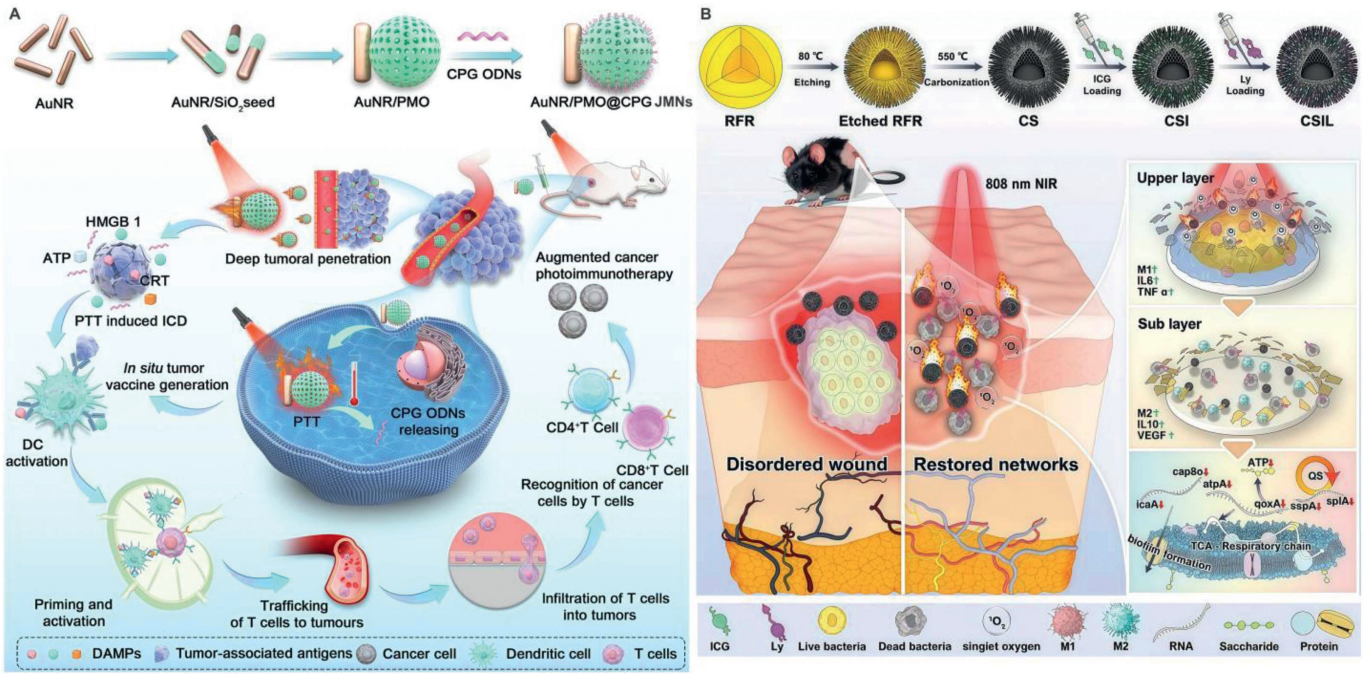


Fig. 5. Schematic diagrams of the light-driven MNMs. (A) Schematic illustration of synthesis of AuNR/PMO@CPG Janus nanomotors and the mechanism for deep tumor delivery, immunosuppressive TME reprogramming and augmented cancer photoimmunotherapy. Reprinted with permission [78]. Copyright 2024, Elsevier Ltd. (B) Schematic illustration of the preparation of the NIR light-driven nanomotor for eradicating MRSA biofilm and promoting wound healing of diabetes through cascade photodynamic therapy (CPDT) strategy. Reprinted with permission [88]. Copyright 2025, Ivyspring International Publisher.

2.3.2. Ultrasound

Ultrasound has been widely used in life sciences due to its non-invasiveness, easy control, excellent tissue penetration ability, and biosafety [91]. When ultrasound propagates in a fluid, it generates a steady-state fluid flow that can drive the movement of MNMs. Additionally, the asymmetric structure of MNMs enables them to undergo self-acoustophoresis. Furthermore, the oscillation or collapse of "cavitation bubbles" produced by ultrasound can also release energy to propel the motion of MNMs. Ultrasound-driven nanomotors can not only use ultrasound to drive motor movement, penetrate deep into tumor tissues, and promote cellular internalization, but also ultrasound-triggered sonodynamic therapy (SDT) can cause ICD, activate anti-tumor immunity, and synergistically enhance anti-tumor treatment [92]. For instance, Ma and coworkers designed an ultrasound-powered piezocatalytic nanomotor, composed of quaternary ammonium chitosan (QCS)/hyaluronic acid (HA) coated Bi_2MoO_6–OH (BMO–OH) loaded with ultrasound-sensitive NOdonor, termed as BQHN (Fig. 6A). Upon activation by ultrasound, BQHN generates NO bubbles and undergoes self-electrophoresis, and the high pressure produced by NO cavitation collapse can further induce piezocatalysis, leading to enhanced self-electrophoresis for dual-mode cascade propulsion. *In vitro* and *in vivo* experiments have demonstrated that the BQHN can achieve efficient tumor penetration and reprogramming of hypoxic TAMs, thereby enhancing the efficacy of cancer immunotherapy [80]. Malthe *et al.* used ultrasound-driven nanomotors to deliver functional Cas9/sgRNA complexes, which are loaded onto the surface of nanomotors through reversible disulfide bonds. A 5-min ultrasound treatment enables the nanomotor loaded with Cas9/sgRNA to directly penetrate the plasma membrane of GFP-expressing B16F10 cells. Cas9/sgRNA is released intracellularly to achieve efficient GFP gene knockout. The acoustic nanomotor loaded with Cas9/sgRNA shows more than 80 % GFP knockout within 2 h after cell incubation, while the knockout using static nanowires is 30 %. Therefore, this intracellular delivery method based on nanomotor provides an attractive approach to overcome the physiological barriers of intracellular delivery of functional proteins and RNA, thus showing great prospects for efficient therapeutic applications [93]. Zhang's group combined nanomotors with O_2 delivery nanocarriers to achieve active intracellular delivery of small gas molecules through nanomotors. Positively charged poly-L-lysine (PLL)-modified Au nanowires (AuNWs) are functionalized with negatively charged red blood cell-perfluorocarbon (RBC-PFC) through electrostatic interaction. In the ultrasound field, the nanomotor rapidly penetrates the cell membrane and continues to move in the intracellular space, and the loaded O_2 is continuously released intracellularly, which helps to maintain cell viability against hypoxia [94]. Chen *et al.* designed a Au-iron oxide nanorod-shaped Janus nanomotor, which accelerates cell internalization under US drive and shows good intracellular movement behavior. The killing efficiency of actively moving nanomotors against cancer cells is 88 % higher than that of static nanomotors, significantly enhancing the induction of cancer cell ferroptosis [95].

Ultrasound-driven nanomotor with Au nanorods modified by model antigen ovalbumin. The rapid movement of the nanomotor facilitates its quick internalization into the cytoplasm of antigen-presenting cells (APCs), enabling APCs activation and cross-presentation of antigens. Meanwhile, the expression levels of MHC class I and MHC class II-related molecules are significantly increased. Compared with traditional passive carrier vaccines, this novel "instant" vaccine delivery strategy based on Au nanowire nanomotors is expected to provide new ideas for developing effective vaccines with enhanced cellular immunity [76]. The same group also designed an acoustic-magnetic responsive nanomotor, which uses superparamagnetic iron oxide NPs as the magnetic "head" and mesoporous silica NPs (MSNs) as the drug carrier to form rod-shaped Janus magnetic mesoporous silica (MMSN) nanomotors (Fig. 6B). The nanomotors are hydrophobically modified with polyethylene glycol (PEG2000) to form MMSN-PEG, and their length is optimized to achieve optimal self-propulsion and intestinal navigation performance. After oral administration, MMSNP can actively direct to the target gastrointestinal site according to

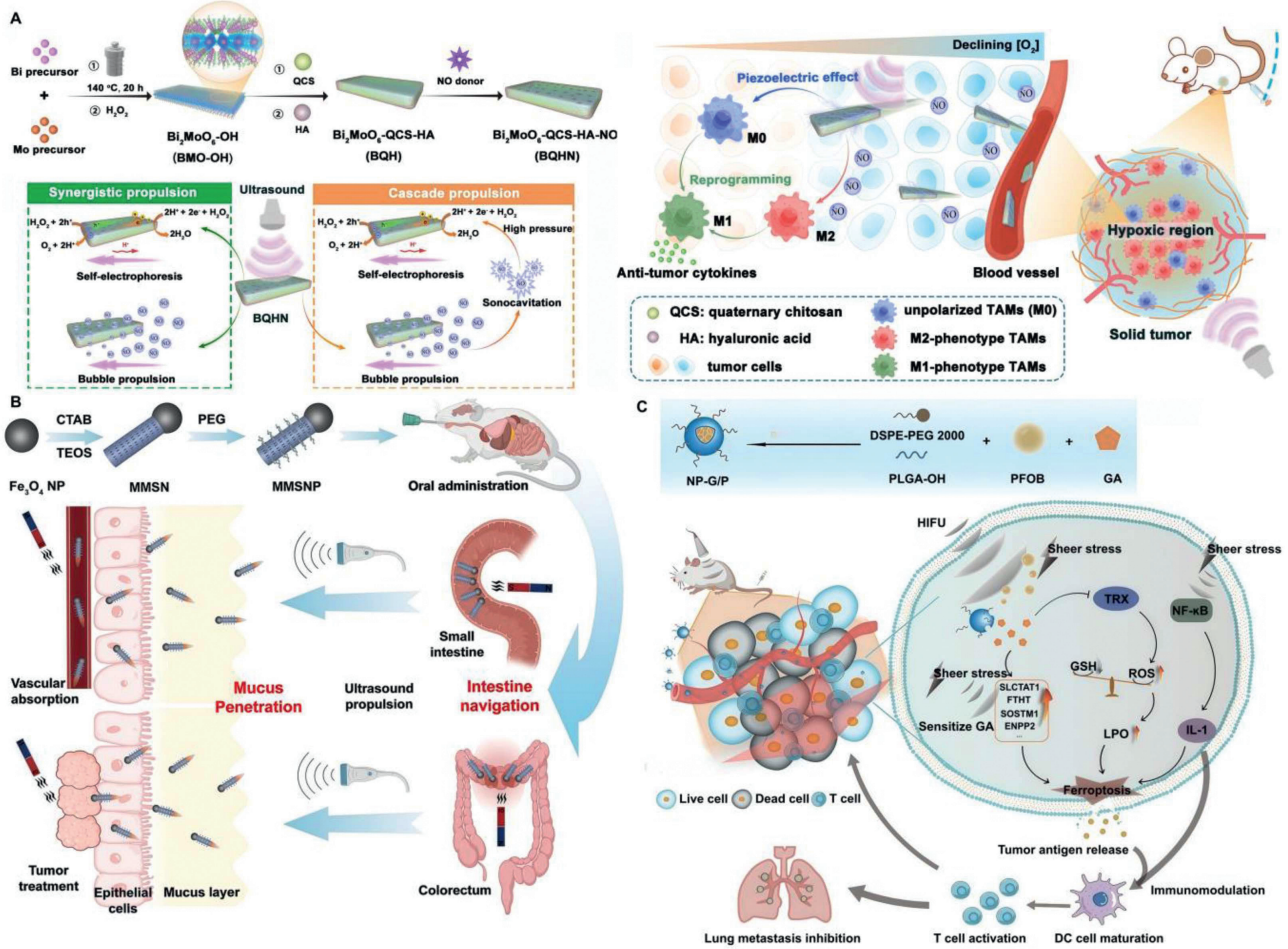


Fig. 6. Schematic diagrams of the ultrasound-driven MNMs. (A) Schematic illustration for the fabrication of BQHN, the mechanism of the dual-modal synergistic/cascade and the penetrating into tumor and reprogramming hypoxic TAMs. Reprinted with permission [80]. Copyright 2025, Elsevier Ltd. (B) Schematic illustration of MMSNP synthesis and the application for the target gastrointestinal site *via* an external magnetic field and effectively penetrate the mucus barrier under ultrasound radiation. Reprinted with permission [81]. Copyright 2025, American Chemical Society. (C) Schematic illustration for the synthetic procedure of nanomotors (NP-G/P) and the antitumor mechanism of HIFU-driven nanomotors on TNBC through improved tumor penetration and robust ferroptosis-immunotherapy. Reprinted with permission [96]. Copyright 2024, Wiley-VCH.

the needs of different diseases. Its highly asymmetric density distribution leads to uneven acoustic pressure distribution within the rod-shaped system, which further promotes the directional movement of the nanomotor, enabling it to actively overcome the intestinal mucus barrier and significantly improve drug delivery efficiency [81]. Yu *et al.* also reported a high-intensity focused ultrasound (HIFU) nanomotor (Fig. 6C). Although the potential mechanism of HIFU-triggered cell death remains unclear, HIFU-induced shear stress may trigger the expression of ferroptosis-related genes including heme oxygenase 1 (HOX1) and glutathione (GSH) S-transferase (GST), making tumor cells sensitive to ferroptosis inducers. It may also induce immune responses against cancer by destroying cancer cells, releasing tumor-specific antigens, and promoting dendritic cell maturation. The HIFU-driven nanomotor targets and delivers ferroptosis inducers to the depth of tumor tissues, enhancing tumor ferroptosis and synergizing immunotherapy. The multifunctional HIFU-driven nanomotor provides a new strategy for precise ferroptosis-based therapy of triple-negative breast cancer [96].

2.3.3. Magnetism

Combined with remotely manipulated magnetic fields, magnetically driven MNMs can actively target specific pathological sites such as tumors and thrombi, rather than relying on random diffusion and systemic circulation [97]. Magnetically driven MNMs remain in the pathological sites for a long time under the control of magnetic fields, thereby providing more efficient treatment and reducing toxic and side effects on normal tissues. For example, Zhou *et al.* designed magnetic silica (SiO_2@Fe_3O_4) NPs, whose surfaces were asymmetrically modified with Pt NPs to enhance the specific surface area and catalytic activity. Studies showed that this nanomotor exhibited superior diffusion capability under low-concentration H_2O_2. Considering the excellent properties of exosomes and their limited targeting ability, the nanomotor was used for targeted exosome delivery. When H_2O_2 concentration similar to that at the tumor site was applied, the delivery of exosomes to breast cancer (MCF-7) cells was significantly enhanced. Additionally, the nanomotor loaded with exosomes and Dox eradicated tumor cells effectively through a dual-targeted delivery system combining magnetic and chemical targeting [98]. Subsequently, Xing's group designed an actin-binding protein-modified magnetic nanomotor (ABP-MN), which features unique magnetism to dynamically respond to magnetic field changes, promoting the conversion of magnetic energy into mechanical energy (Fig. 7A). It induces F-actin depolymerization in a non-invasive, highly penetrative, and remotely controlled spatiotemporal manner, leading to contraction and damage of tumor cells and cancer-associated fibroblast (CAF) cells. This reduces tumor stroma stiffness and remodels the tumor mechanical microenvironment [82]. An *et al.* also designed a magnetically con-

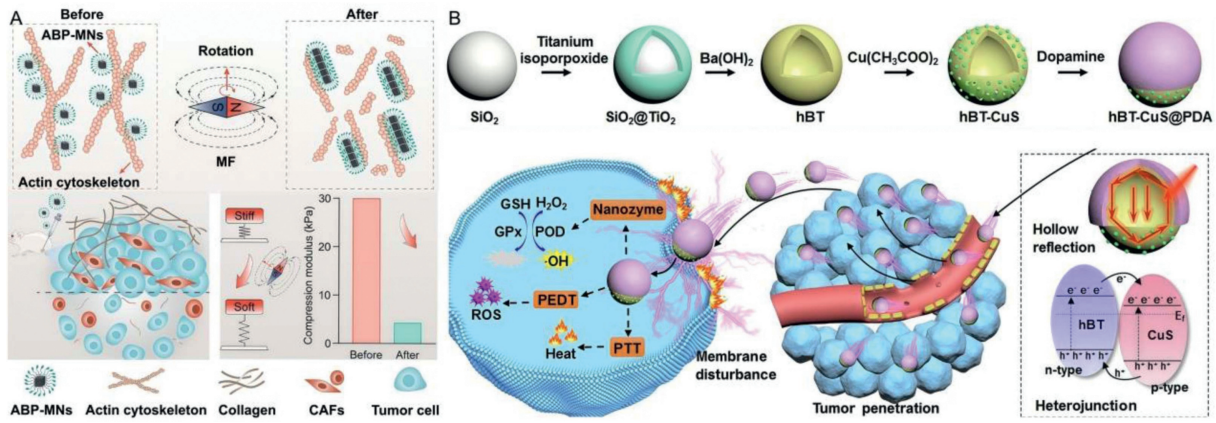


Fig. 7. Schematic diagrams of the ultrasound or electrically driven nanomotors. (A) Schematic illustration intracellular mechanical regulation of the actin cytoskeleton by actin-binding protein-modified magnetic nanomotor under magnetic field to reshape the tumor mechanical microenvironment. Reprinted with permission [82]. Copyright 2025, American Chemical Society. (B) Schematic illustration of hBT-CuS@PDA preparation and working mechanism, thermophoresis-driven motion and pyroelectric field promote NP accumulation and diffusion in tumors and internalization into tumor cells. Reprinted with permission [84]. Copyright 2024, Elsevier Ltd.

trolled and chemically driven nanomotor tablet that can actively retain in the gastrointestinal tract (GI tract). The micro-motor pill is propelled toward the target area in the intestine by an external low-frequency gradient alternating magnetic field. The high-frequency alternating magnetic field induces strong water-driven propulsion in the micro-motor *via* magnetothermal effects, effectively prolonging its residence time in the intestine. This provides a novel strategy for active drug delivery in gastrointestinal therapy [99].

Another example is Liu *et al.* synthesized a novel magnetic mesoporous silica/ε-polylysine nanomotor-based remover (MMS/P NR) with abundant chelating sites. The magnetic core enables the nanocomposite to act as an autonomous nanomotor under an external alternating magnetic field, significantly increasing the contact probability between MMS/P NRs and Pb^{2+}-contaminated hemoglobin (Hb) in red blood cells. Amino-rich ε-polylysine (ε-PL) serves as a co-template for mesoporous silica, and the mesoporous channels provide a confinement effect for Pb^{2+}-contaminated Hb, stably capturing Pb^{2+} in blood. This nanomotor-based remover design strategy holds great potential for future medical treatment of heavy metal poisoning [100].

Qiu *et al.* designed asymmetric multilayer sandwich magnetic mesoporous silica nanobottles (MMSNBs), with single layers of Fe_3O_4 NPs uniformly assembled on the inner and outer surfaces, endowing them with high magnetization. The mesoporous silica layer features a large surface area and pore size. By integrating CAT, a novel CAT-driven nanomotor is obtained. CAT deactivates in the presence of specific pollutants, enabling monitoring of water contaminants. Once heavy metal ions are detected, MMSNBs act as excellent adsorbents for pollutant removal. The Fe_3O_4 component enables directional movement under a magnetic field, and MMSNBs are recyclable [83].

2.3.4. Electricity

Electric field-driven MNMs can move by means of self-electrophoresis, or they can generate ion concentration gradients or gases through electrochemical reactions on the surface of the MNMs to propel themselves into motion. Electric field-driven MNMs can be combined with electric field-based therapies. Electrotreatment, as an emerging and promising research direction in tumor therapy, offers synergistic advantages of deep tissue penetration, spatiotemporal selectivity, and low systemic toxicity [101]. High-voltage electric pulses can disrupt cell membranes to inhibit bacterial growth. Meanwhile, electric fields can induce microelectrolysis of water and generation of ROS, avoiding drug resistance issues (Fig. 7B). Pyroelectric materials exhibit dipole displacement and spontaneous polarization in response to temperature changes, generating electrons and holes that produce ROS for pyroelectric therapy (PEDT) [84,102].

Based on this, Meng *et al.* prepared Janus-type tBT@PDA NPs by partially coating pyroelectric tetragonal barium titanate (tBT) NPs with PDA caps, then loading ciprofloxacin (CIP) onto the PDA caps to obtain tBT@PDA-Cip NPs. NIR irradiation of the PDA layer generates a photothermal effect to drive NPs movement and induces a pyroelectric effect on tBT NPs, enhancing CIP release and antibacterial photothermal dynamic therapy. The built-in pyroelectric field on the NPs disrupts bacterial membrane potential, increasing membrane fluidity and permeability to enhance bacterial uptake of CIP, synergistically boosting antibacterial treatment [103].

The diffusion of drugs in tumor tissues and the internalization by tumor cells are key issues affecting antitumor efficacy. External electric fields strongly influence cell membrane polarization and fluidity but often require complex circuit devices. Developing nanomotors that generate *in-situ* microelectric fields addresses these challenges. Meng's group designed Janus-type tBT@PDA-CPT NPs by partially coating pyroelectric tBT NPs with PDA caps and linking camptothecin (CPT) *via* disulfide bonds, using non-pyroelectric cubic barium titanate cBT@PDA-CPT NPs as a control. NIR irradiation of the PDA caps of Janus NPs produces asymmetric thermophoretic forces to drive NPs movement, enabling tumor enrichment, deep tissue penetration, and effective cell interactions. PDT induced temperature changes on tBT NPs establish pyroelectric potentials, selectively altering the membrane potential of tumor cells rather than normal cells, playing a dominant role in enhancing tumor cell internalization and cytotoxicity. This achieves complete inhibition of tumor growth and significantly prolongs animal survival time [104]. The combination of electric field-driven nanomotors and electrotherapy can precisely and efficiently enhance the therapeutic effect. The deep delivery capability of nanomotors enables the electric field therapy to be accurately controlled and activated after reaching the target site, which embodies the low toxicity of the design.

2.4. Hybrid-driven MNMs

Nanomotors can convert various energies (chemical, light, acoustic, *etc.*) into kinetic energy for movement. Compared with single-driven nanomotors, hybrid-driven nanomotors integrating multiple propulsion mechanisms into a single motor enhance their robustness in complex environments and reduce dependence on

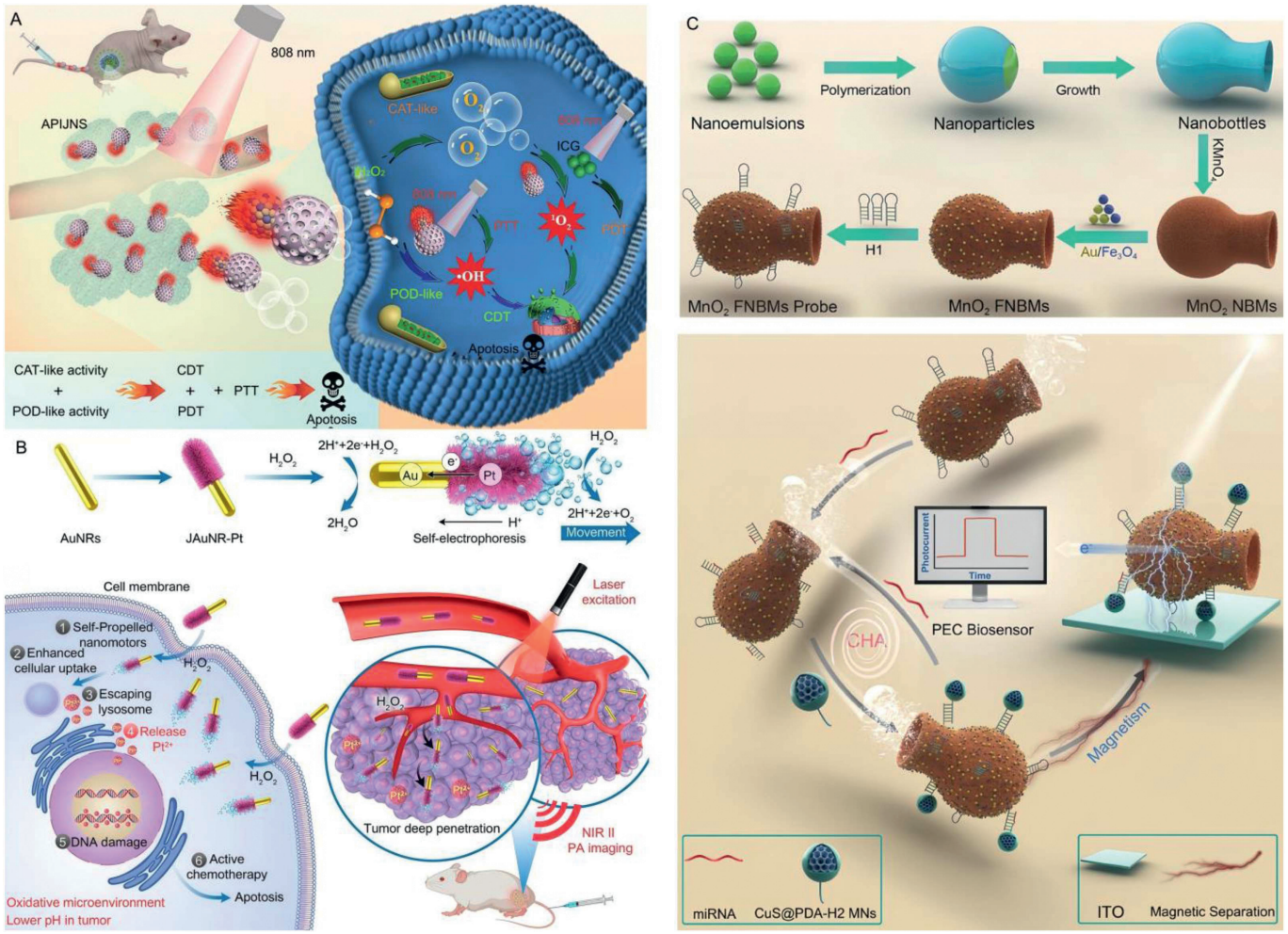


Fig. 8. Schematic diagrams of the hybrid driven nanomotors. (A) Schematic illustration of dual-source driven parachute-like Janus nanomotor, which catalyze H_2O_2 to achieve autonomous drive and form photothermally induced self-thermophoresis drive, achieving better synergistic CDT/PTT/PDT. Reprinted with permission [105]. Copyright 2024, Wiley-VCH. (B) Schematic illustration of the synthesis route of the JAuNR-Pt nanomotor and their application for NIR-II PA imaging of deep tumor tissues and antitumor effect. Reprinted with permission [106]. Copyright 2022, American Chemical Society. (C) Schematic illustration of the preparation of a nanomotor probe and the fabrication the PEC biosensor for the detection of miRNA. Reprinted with permission [107]. Copyright 2024, Wiley-VCH.

fuel resources or other environmental parameters. However, each driving mode is based on specific principles and control mechanisms. Designing intelligent nanomotors that can actively respond to external stimuli and coordinate these propulsion modes to achieve synchronous operation remains a significant challenge.

To cope with this challenge, Zhang *et al.* prepared a dual-driven parachute-shaped Au_2Pt@PMO@ICG Janus nanomotor (APIJNS) to improve deep tumor penetration, alleviate tumor hypoxia, and enhance the synergistic effect of PTT/CDT/PDT (Fig. 8A). APIJNS exhibits high catalytic POD-like/CAT-like activity and photothermal effects, efficiently catalyzing H_2O_2 to generate abundant ROS for autonomous driving while inducing photothermal-driven self-thermophoresis, achieving triple synergistic therapy of PTT/PDT/CDT [105]. Lv and co-workers studied a hydrogenated titanium dioxide (H-TiO_{2-x}) Janus mesoporous nanomotor for enhanced tumor penetration and NIR-light-triggered PDT. The nanomotor consists of NIR-responsive H-TiO_{2-x} nanospheres and CAT-modified periodic mesoporous organosilica (PMO) nanorods wrapped around them. Movement is driven by CAT decomposing overexpressed H_2O_2 in the TME into O_2 and H_2O, and by H-TiO_{2-x} converting 808 nm laser energy into heat. Additionally, H-TiO_{2-x} subunits convert O_2 to harmful $^1O_2$, inducing intracellular oxidation and apoptosis. Excess endogenous H_2O_2 is continuously decomposed *via* enzymatic reactions to replenish O_2 consumed in PDT, enabling potent PDT [108].

Li and collaborators developed a H_2O_2-driven Janus Au nanorod-Pt (JAuNR-Pt) nanomotor, which actively penetrates deep tumor tissues and continuously releases Pt^{2+} ions for effective tumor treatment (Fig. 8B). Constructed by depositing a Pt nanoshell on one end of Au nanorods, it exhibits strong NIR-II PA imaging signals. In the presence of H_2O_2, direct contact between Au nanorods and the Pt nanoshell enables electron transfer, driving rapid autonomous movement. NIR-II PA imaging confirms enhanced tumor penetration and excellent therapeutic efficacy [106]. Zhang and co-workers prepared a dual-driven spindle-shaped Janus nanomotor (Pt/FePc@Mn-MOF), which catalyzes endogenous H_2O_2 decomposition to generate O_2 bubbles, relieving TME hypoxia and driving the nanomotor. Pt/FePc@Mn-MOF shows dual peroxidase-like and oxidase-like activities, producing abundant ROS. NIR light triggers self-thermophoresis and PTT, while Mn-MOF consumes GSH *via* redox reactions, releasing Mn^{2+} for Mn^{2+}-based CT imaging to guide antitumor therapy [109].

A dual-responsive manganese dioxide-loaded carbonaceous nanobottle motors (MnO_2 NBMs) were developed *via* interface assembly, which exhibit self-diffusiophoresis and self-thermophoresis in response to H_2O_2 and NIR light, respectively

(Fig. 8C). Assembling nanomotors with functional NPs and hairpin DNA (hDNA) constructs swimmable functional MnO_2 NBMs (MnO_2 FNBMs) probes, which move around complex samples to improve target miRNA transport, accelerate receptor-target interactions, and enhance detection range and speed [107].

The above section elaborates on the design strategies of intelligent nanomotors with different driving modes. (1) The preparation of bio-driven nanomotors utilizing the chemotaxis of cells and simple organisms features excellent biocompatibility, which embodying the environmentally friendly design concept. (2) The zero-waste self-destructing nanomotors, which utilize endogenous biofuels (such as glucose and lactic acid) to generate gas for promoting the deep penetration of nano-drug delivery systems and improving the environment of the treatment site, reflect the design concept of turning waste into treasure. (3) The utilization of external green and clean energy sources, which are converted into kinetic energy for the movement of the motors and synergized with PTT, PDT or SDT to achieve efficient and controllable treatment, embodies the design concept of efficient energy utilization and biosafety.

3. Applications of MNMs in biomedical field

MNMs exhibit excellent active movement capabilities, enabling efficient and precise drug delivery to pathological sites while avoiding toxicity on normal tissues. They can absorb external energy to enhance deep tissue penetration and synergize with therapies such as chemotherapy, PTT, PDT, SDT and immunotherapy, achieving "one stone, two birds" effects. This aligns with the design objectives of resource optimization and efficient treatment.

3.1. Cancer

Cancer is a major disease threatening human health. Abnormal vascular structures in tumor tissues, high interstitial pressure, and the dense ECM in the TME restrict the intratumoral penetration and cellular internalization of nanomedicines. Most tumors also feature drug resistance and high metastasis potential. Therefore, constructing nanomotors capable of deep tumor tissue penetration can overcome these limitations.

Based on the higher H_2O_2 content in tumor tissues than in normal tissues, Hu *et al.* designed a NIR light-driven self-thermophoretic nanomotor capable of catalyzing H_2O_2. By asymmetrically coating PDA on zinc dioxide NPs, and then chelating ferrous ions using the polyphenol groups in the PDA coating, a Janus-type zinc dioxide@PDA-iron (Z@P-F) nanomotor was successfully prepared. The asymmetric PDA shell absorbs NIR light to form a thermal gradient around the nanomotor. In the acidic TME, Z@P-F continuously generates a large amount of lipid ROS and consumes GSH in tumors by releasing ferrous ions and H_2O_2, efficiently inducing ferroptosis and improving antitumor efficacy [110]. In addition, Wang *et al.* also utilized the physiological characteristics of the weak acidic TME, high H_2O_2 and GSH concentrations to design a charge-reversing nanomotor. The nanomotor is composed of 3,4,5,6-tetrahydrophthalic anhydride (TA)-modified DOX-loaded mesoporous organosilica Pt (DOX/MSN-Pt@TA). The negatively charged surface of the nanomotor promotes the *in vivo* circulation of NPs, which accumulate in tumor tissues through the EPR effect. β-Carboxamide bonds break in the weak acidic TME, causing the NPs to reverse their charge. The Pt catalyzes the highly expressed H_2O_2 in tumor tissues, and synergizes with the positive charge on the NPs surface to penetrate tumor tissues. DOX is released due to the degradation of mesoporous silica in response to highly expressed GSH, effectively eliminating tumors [111]. In the above example, the driving of the MNMs relies on endogenous substances in the TME, without the need for additional introduction of external fuels. MNMs can degrade in response to the TME, which are "reducing the introduction of harmful substances" and "avoiding the metabolic residues of harmful substances".

Cisplatin (CDDP), due to its broad-spectrum antitumor activity, is a first-line drug for treating various cancers [112]. It inhibits DNA replication by binding to cellular DNA, leading to tumor cell apoptosis. However, due to tumor cell drug resistance, clinical use of high-dose CDDP causes nephrotoxicity, neurotoxicity, and other side effects [113]. Xu *et al.* designed an H_2O_2-driven CDDP-loaded nanomotor to enhance its therapeutic efficacy and reduce side effects (Fig. 9A). Specifically, tannic acid (TA) and poloxamer 188 (F68) were used as two self-assembling building blocks for CDDP delivery. Additionally, silver NPs were *in-situ* deposited on the polymer side loaded with CDDP to prepare an asymmetric nanostructure (AINR). The Janus-structured AINR achieves autonomous movement driven by H_2O_2 in tumor tissues, where H_2O_2 is catalytically decomposed by silver NPs into abundant O_2 bubbles. The local concentration gradient of O_2 bubbles drives the drug to penetrate deeper into tumor tissues. The uniformly distributed nanocarriers in tumor tissues are rapidly internalized by tumor cells *via* endocytosis, inducing potent CDDP-based tumor chemotherapy [114]. MNMs, driven by their responsiveness to the TME, can enhance the accumulation of drugs at tumor sites and reduce the overall administration dosage. Thus, decreases the non-specific distribution of drugs in the body, representing the "low toxicity and safety".

Ye's group prepared ultrasound-driven Janus NPs with partially coated Au nanorods and mesoporous silica for deep tumor penetration. Under ultrasound, 2,2-azobis[2-(2-imidazolin-2-yl)propane]dihydrochloride loaded in silica generates nitrogen microbubbles to drive the nanomotor. Due to the deep penetrability of ultrasound, the nanomotor can move in the deep tumor tissue and enhance the PA imaging effect inside the tumor. The synergy between nitrogen and SDT provides a new strategy for precise tumor treatment [115].

GBM is a primary brain tumor derived from glial cells [116]. The BBB makes it difficult for therapeutic drugs to be effectively delivered to the tumor site, and the dense microenvironment of the tumor tissue makes it difficult for drugs to deeply penetrate into the tumor to exert their efficacy [117]. Therefore, GBM is a huge challenge in cancer treatment. Ye and co-workers designed a photothermal and bubble dual-driven nanomotor (HM@MnO_2-AuNR-SiO_2) modified with biomimetic hybrid cell membrane (HM) for targeted GBM treatment (Fig. 9B). HM is formed by fusing glioma cell membrane (homologous tumor targeting ability) and macrophage membrane (enhanced BBB crossing ability), which can actively target and accumulate in the glioma area of the brain. MnO_2 can convert H_2O_2 into O_2, and bubbles drive the movement of the motor. AuNR has strong absorption in the NIR II region, which can carry out photothermal conversion and generate a significant thermal gradient on the nanomotor, enabling the nanomotor to move actively and effectively treat the deep GBM tumor site. The AuNR-MnO_2 heterostructure can promote the separation of electron-hole pairs and generate a large number of ROS through plasma-enhanced catalytic activity, thereby inducing ICD in tumors. MnO_2 can react with GSH in the TME, release Mn^{2+} *in situ*, activate the STING signaling pathway, trigger a strong immune response, improve the efficacy of tumor immunotherapy, and achieve efficient eradication of GBM [118]. Li and collaborators designed a chemotactic nanomotor with GOx and carboxylated CDDP prodrug loaded on L-arginine-derived polymer. The nanomotor has chemotaxis to inducible NOS and ROS highly expressed in the GBM microenvironment. NO generated by L-arginine decomposition and glucose decomposition dual-drive the movement of the

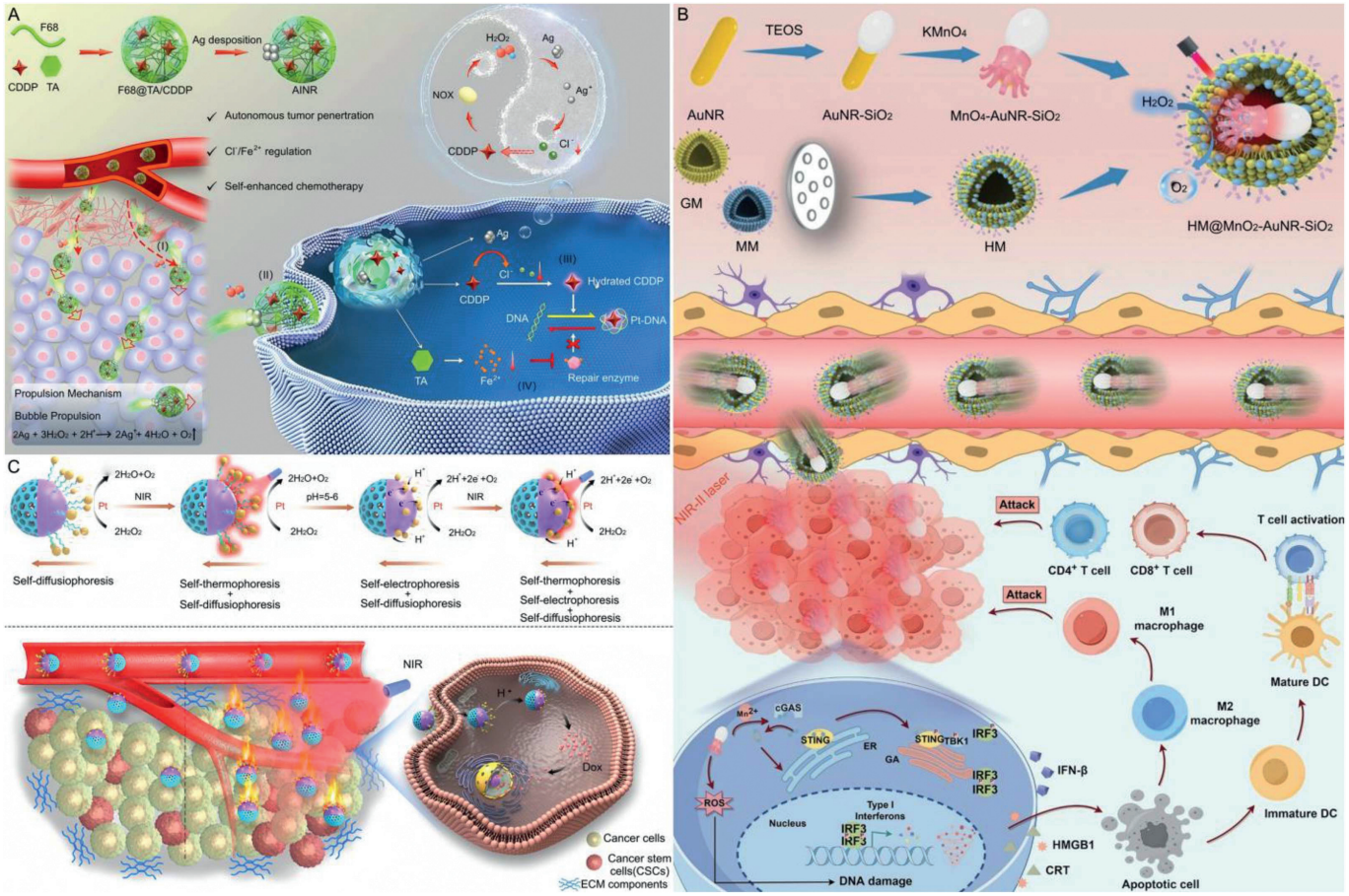


Fig. 9. Schematic diagrams of the nanomotors for cancer treatment. (A) Schematic illustrations of construction of AINR and the action mechanisms of AINR for boosting CDDP chemotherapy. Reprinted with permission [114]. Copyright 2022, BioMed Central. (B) Schematic diagram of the fabrication process for the HM@MnO_2-AuNR-SiO_2 nanomotor and its enhancing antitumor immune response *via* ROS generation and STING pathway activation for targeted GBM therapy. Reprinted with permission [118]. Copyright 2025, Wiley-VCH. (C) Schematic illustration of the JMSNs@Pt@P-Au nanomotors enhance deep tumor penetration and drug delivery *via* multi-propulsion for CSCs-targeted cancer therapy. Reprinted with permission [120]. Copyright 2025, Elsevier Ltd.

motor. NO, loaded GOx and CDDP can play the combined role of NO/starvation/chemotherapy, induce enhanced immune response through multiple pathways, and better cope with the complexity of GBM treatment [119].

For the treatment of cancer stem cells (CSCs) deep in tumors, there is a problem that nanomedicines mainly accumulate on the tumor surface, and ordinary nano-drug delivery systems are difficult to cross cell and tissue barriers, limiting the therapeutic effect [121]. Zhang *et al.* designed a pH-responsive Janus mesoporous silica Pt-Au nanomotor with multiple propulsion forces (Fig. 9C). In a neutral microenvironment, Au NPs and Pt NPs remain separated. Asymmetrically deposited Pt catalyzes H_2O_2 to generate O_2, forming a concentration gradient on one side to drive nanomotor movement *via* self-diffusiophoresis. Upon reaching the tumor site, the acidic microenvironment triggers shrinkage of poly(methacrylic acid) (PAA) molecular brushes, promoting contact between Au and Pt NPs. This contact induces electron transfer in H_2O_2 solution, creating an electron concentration gradient that drives nanomotor movement *via* self-electrophoresis. Additionally, under NIR irradiation, asymmetric Au NPs generate thermal gradients to drive the nanomotor *via* self-thermophoresis. Due to the asymmetric Janus structure, these multiple propulsion forces collectively drive the nanomotor toward the silica shell side. The three propulsion modes enable DOX delivery to deep tumor regions, where chemotherapy synergizes with PTT to kill CSCs, providing a novel strategy for CSC treatment [120]. Harnessing the "endogenous characteristics" of the TME to achieve targeted functions and responsive activation can reduce toxic and side effects, exhibit better biocompatibility, promote the efficient utilization of drugs, and synergistically enhance anti-tumor efficacy.

Gene-editing-based tumor therapy holds broad prospects, but traditional passive diffusion carriers have limited penetration in dense solid tumors. Liu *et al.* designed a ROS -driven gene-editing nanomotor self-assembled from amphiphilic oligomers of chitosan-hemin (Cs-He) and chitosan-palmitic acid (Cs-Pa). Engineered to actively target tumor cells under ROS gradient induction, it enables efficient cargo delivery, cellular uptake, and lysosomal escape. Hemin rapidly degrades extracellular ROS, alleviating immunosuppression of ICD caused by extracellular ROS accumulation. Upon cellular uptake, hemin is catabolized by heme oxygenase-1 (HO-1) overexpressed in tumor cells to generate CO, triggering plasmid-responsive release. CRISPR/Cas9 proteins knockout the LDHA locus, inhibiting tumor cell glycolysis, enhancing mitochondrial activity, and inducing intracellular ROS burst. Reduced LDHA expression decreases lactate in tumor cells, relieving immune microenvironment suppression. Additionally, endogenous CO promotes endothelial cell growth, normalizes tumor vasculature, and optimizes the immune microenvironment, achieving tumor metabolic intervention and enhanced immunotherapy. This nanomotor provides a new option for CRISPR/Cas9 targeted delivery and tumor therapy [122].

The examples shown above illustrate the application of MNMs in cancer therapy. This includes designing MNMs based on the unique microenvironment of tumor tissues for anti-tumor ther-

apy. The MNMs drug delivery system enhances the efficacy of the first-line anti-cancer drug, CDDP, and reduces its side effects. By combining with photoacoustic imaging, MNMs enable precise visualized treatment of tumors. Nanomotors can improve the therapeutic effect on deep-seated tumors such as gliomas. Additionally, MNMs can be combined with immunotherapy, stem cell therapy, and gene therapy to synergistically enhance anti-tumor efficacy. MNMs hold the significant potential in future biomedicine. However, most MNMs structures rely on metallic materials or functional polymers, some of which inherently pose potential toxicity. Additionally, MNMs struggle to maintain stable movement consistently *in vivo*, and their lack of targeting ability remain key issues that need to be addressed.

3.2. Cardiovascular diseases

Thrombosis, a life-threatening major complication of cardiovascular diseases, contributes to one-fourth of global deaths [123]. Current treatments face challenges: thrombolytic drugs have short half-lives, requiring frequent high-dose administration that causes significant side effects; drug injection lacks targeting, with only 5 % of drugs reaching the lesion; and drugs remain on the thrombus surface, failing to penetrate internally for ideal efficacy [124].

For example, Fang *et al.* designed and prepared PDA nanomotors modified with arginine-glycine-aspartic acid (RGD) peptides and loaded with thrombolytic drug urokinase (UK). RGD targets the thrombus site to release UK. Under NIR light irradiation, PDA converts light energy into heat to drive nanomotor movement. The guanidyl group of arginine in RGD interacts with ROS in the thrombus microenvironment to generate NO, which not only propels the motor but also promotes vascular endothelial cell growth to repair damaged vessels. The NIR-light and NO dual-driven nanomotors enable continuous deep penetration into thrombi, achieving synergistic photothermal and drug therapy [127]. Wan's group developed mesoporous/macroporous silica (MMS)/Pt nanomotors coated with platelet membranes (PM). The macroporous structure of the nanomotors loads thrombolytic drug UK, while the mesoporous structure loads anticoagulant heparin. PM targets the nanomotors to thrombi (Fig. 10A). The uneven distribution of Pt and its photothermal conversion generate self-thermophoretic force to drive motor movement, allowing MMNM/PM nanomotors on the thrombus surface to penetrate into the thrombus interior. Photothermal effects enable controlled drug release, increasing the penetration depth and retention rate of the nanomotor drug delivery system at the thrombus site to prevent recurrence [125].

Su *et al.* prepared a nanomotor drug delivery system (APBUL) for thrombolytic therapy, which consists of fibrin-specific peptide CREKA-modified thermosensitive liposome-encapsulated nanobowls composed of Au-Pt NPs and loaded with UK. The CREKA peptide can specifically target the thrombus site. Under NIR irradiation, the thermosensitive liposomes rupture to release UK and Au-Pt NPs. The asymmetric structure of Au-Pt NPs enables self-thermophoretic movement, achieving PTT while penetrating deeper thrombus tissues. Pt NPs have CAT-like ability to catalyze H_2O_2 to produce O_2, reducing oxidative stress at the thrombus site and decreasing the level of inflammatory factors. In addition, combining the treatment method with photoacoustic imaging can not only reduce the drug dosage but also improve the real-time monitoring of disease treatment [128]. Zhang and coworkers prepared a thermo-gas dual-driven "thrombin-NIR" dual-responsive nanomotor (Pep-NO@PPC/UK). CREKA mediates the targeting of nanomotors to the thrombus site. PDA converts NIR light into heat and simultaneously triggers NO release (Fig. 10B). The "thermo-gas" dual-propelled nanomotor drives the deep penetration and uniform distribution of UK in the thrombus. Under the combined action of UK and PTT, arterial thrombi are rapidly dissolved [126]. Ruan's group developed a NIR/ultrasound-triggered targeted nanomotor, which encapsulates ferrous oxide NPs (Fe_3O_4 NPs), perfluorohexane (PFH), and UK into liposomes. Through magnetic field navigation, the nanomotors aggregate on the surface of the thrombus. PFH rapidly heats up under NIR and ultrasound stimulation to achieve thermotherapy thrombolysis. As the temperature rises, the loaded PFH undergoes liquid-gas phase transition, and relatively non-invasive ultrasound thrombolysis is achieved through cavitation effect, so as to realize the multi-stage propulsion cascade strategy treatment and multimodal imaging diagnosis of venous thrombosis [129].

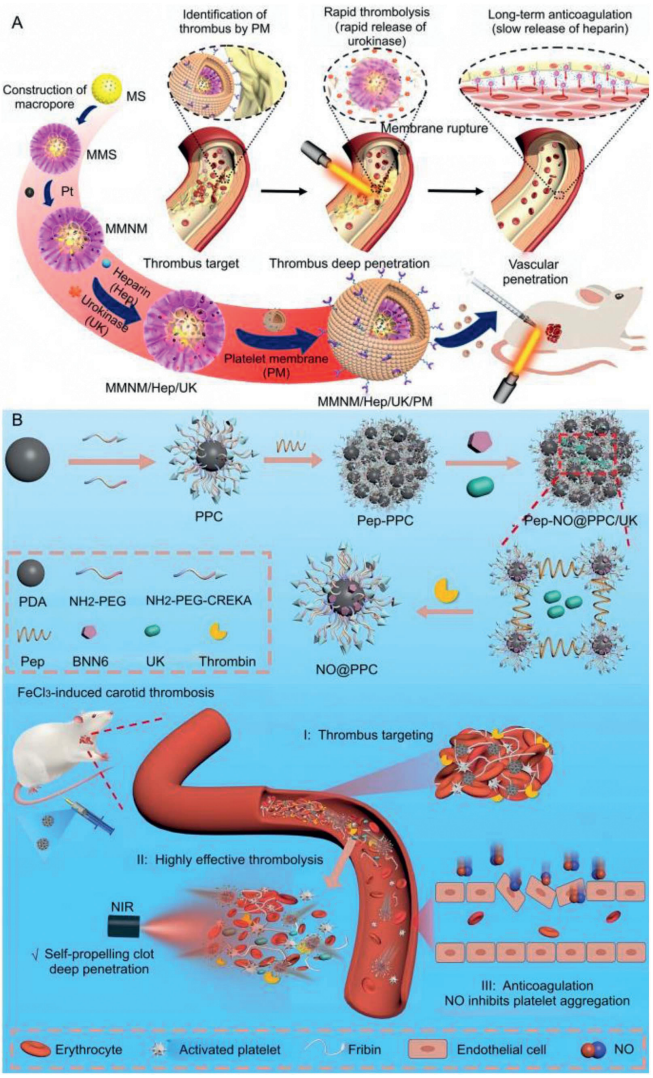


Fig. 10. Schematic diagrams of the nanomotors for thrombus therapy. (A) Schematic illustrations of the fabrication of MMNM/Hep/UK/PM nanomotors and their application for thrombus targeting and thrombolytic treatment. Reprinted with permission [125]. Copyright 2020, American Association for the Advancement of Science. (B) Schematic diagram of the synthetic route and thrombolysis mechanism of Pep-NO@PPC/UK. Reprinted with permission [126]. Copyright 2024, Elsevier Ltd.

Nanomotor-driven mechanical therapy also holds certain potential for thrombus treatment [130]. Xia *et al.* designed a phosphatidylcholine (PC) liposome-coated accelerated Pt nanomotor (Pt@PDA@Lipo, PLANE). Pt catalyzes the decomposition of H_2O_2 to generate O_2, driving the nanomotor movement. The hydrated surfactant headgroups of PC lipids form an interface to reduce friction at the solid-liquid interface, while the isotropic surface of PC liposomes helps mitigate tortuous motion, enabling linear move-

ment and increasing the swimming speed of PLANEs. Additionally, PDA serves as a structural support for Pt nanomotors and exhibits excellent photothermal properties for photothermal thrombolysis. To enhance thrombus targeting, the surface of PLANEs was functionalized with cysteine-arginine-glutamate-lysine-alanine (CREKA) peptide, which specifically binds to fibrin, increasing the accumulation of PLANEs at the thrombus site and improving the efficacy of mechanical therapy. This optimization of Pt nanomotor motility provides a promising non-drug approach for thrombus disease treatment [131].

Researchers select biocompatible materials (such as polypeptides and liposomes) to construct MNMs. The construction process is green and environmentally friendly. Clean energy sources like light energy and ultrasound are used to drive the movement of the motors, enabling precise control over the movement of nano motors. In combination with photothermal or ultrasonic therapy, they can synergistically and efficiently ablate thrombi with drugs. In the future, the optimization and upgrading of driving methods, as well as the integrated design of diagnosis and treatment, can promote the translation of nanomotors from the laboratory to clinical practice.

3.3. Wound healing

Delayed or non-healing diabetic wounds can trigger diabetic nephropathy and cardiovascular complications [132]. In clinical practice, the combined use of antibiotics and hypoglycemic drugs is a common method for treating infected diabetic wounds, but it suffers from off-target effects, bacterial resistance, and blood glucose fluctuations. Hu and co-workers designed a glucose-fueled cationic nanomotor that enables active targeting of bacterial-enriched areas. Composed of mesoporous dopamine NPs, the nanomotor loads GOx and CAT, uses glucose at physiological concentrations in diabetic wounds as fuel, and exhibits chemotaxis toward tissues with high glucose and H_2O_2 levels. Leveraging the high glucose concentration and H_2O_2 levels during bacterial proliferation and metabolism in wounds, it achieves targeted accumulation, bactericidal activity, and hypoglycemic effects in bacterial-enriched regions [133]. Lin *et al*. also designed a GOx- and CAT-modified mesoporous silica nanomotor powered by endogenous glucose in diabetic wounds (Fig. 11A). *In vivo* experiments showed that after spray administration, the pre-modeled wounds of diabetic mice healed nearly 30% faster than the control group, with significantly reduced inflammation and ROS levels and increased vascular endothelial growth factor levels [134].

Hyperglycemia causes vascular blockage, restricting the smooth delivery of O_2 and nutrients to wounds and disrupting the healing process [135]. Additionally, hyperglycemia prone to bacterial infection weakens the immune system's bactericidal ability and exacerbates wound inflammation. Xie and collaborators designed an O_2 and NO-driven nanomotor by asymmetrically coating CaO_2 NPs with PDA, complexing with Fe^{2+}, and grafting cysteine-NO (CNO) on the PDA layer to obtain Ca@PDAFe-CNO NPs. CaO_2 decomposes to generate O_2, driving NPs diffusion in biofilms, while the produced H_2O_2 and Fe^{2+} serve as raw materials for the Fenton reaction to generate $^{\bullet}OH$. CNO grafts react with GSH at the wound site to release large amounts of NO, enhancing endothelial cell migration, angiogenesis, and collagen deposition during wound healing, thus accelerating wound healing in diabetic patients [136].

Diabetic wounds also contain high levels of lactate [137]. Zheng *et al*. demonstrated a cascade-driven DMSNs-Pt-LOX@Nisin nanomotor, where LOX loaded on DPLN exhibits high catalytic activity toward elevated lactate levels common in diabetic wounds, generating fuel H_2O_2. Unilateral Pt nanostructures then catalyze H_2O_2 decomposition to produce O_2, enabling autonomous propulsion of the nanomotor. Both *in vitro* and *in vivo* experiments confirm that DPLN accelerates wound healing by promoting cell migration, angiogenesis, and reducing inflammatory responses [138].

Wang *et al*. developed a dual-targeted nanoplatform where enzymatic catalysis of cerium dioxide (CeO_2) NPs generates O_2 for deep penetration (Fig. 11B). As a potent ROS scavenger, CeO_2 NPs alleviate the highly oxidative inflammatory wound microenvironment, promoting local macrophage polarization from pro-inflammatory M1 to anti-inflammatory M2 phenotypes, offering a novel strategy for chronic wound healing with bacterial infection [139].

By leveraging the unique microenvironment of wounds (such as high glucose and lactic acid levels, hypoxia), MNMs fueled by glucose and lactic acid are constructed. The MNMs can generate O_2 to improve the hypoxic environment, thereby turning "waste" into "treasure" and achieving precise and efficient therapeutic effects. Wound healing is a complex, dynamic process that unfolds across multiple stages, and its treatment requires the simultaneous achievement of multiple goals, such as "efficient antibacterial activity, precise anti-inflammation, and promotion of tissue repair". However, the inherent physiological barriers of wounds and changes in the dynamic microenvironment significantly impair the targeted enrichment efficiency and deep tissue delivery capability of MNMs. These critical issues urgently await exploration and breakthroughs in future research.

3.4. Antibacterial

Bacterial infection is an increasingly severe global issue. Antibiotics are the most commonly used antibacterial agents, but they suffer from drug resistance [140]. Nanomaterials generally exhibit multiple antibacterial mechanisms, making it difficult for bacteria to develop resistance, yet their efficacy is limited by insufficient bacterial contact [141]. MNMs possess self-propulsion capabilities, and their active movement significantly enhances interactions and adhesion with bacteria. Additionally, the efficient delivery of antibacterial agents *via* active transport mechanisms strengthens antibacterial activity. Kiristi and collaborators designed ultrasound-driven nanomotors modified with multiple lysozymes. Under an ultrasonic field, the nanomotors increase the interaction between lysozymes and bacteria, demonstrating higher antibacterial activity compared to static NPs. This novel antibacterial nanomotor strategy provides efficient and rapid bactericidal capability, embodying the efficient and environmentally friendly applications of green chemistry [142].

Li and co-workers constructed a jellyfish-like mesoporous PDA ($PDA\text{-}NH_2$@Ag) nanomotor loaded with silver NPs, which exhibits rapid autonomous movement under NIR light irradiation, accelerating contact with bacteria. The photothermal-induced temperature increase and the efficient antibacterial activity of Ag NPs synergistically enhance the antibacterial effect [143]. Guo *et al*. reported a photocatalytic MNMs based on liquid metal (LM). The prepared Ga-based LM micro/NPs are modified with g-C_3N_4 nanosheets on one side and coated with a thin layer of Pt on the other side (Fig. 11C). The MNMs show active self-electrophoretic propulsion in low-concentration H_2O_2 solutions, and the application of light further enhances their motility. The charge separation amplified by LM contributes to the efficient generation of ROS, which act as strong oxidants to effectively eradicate bacteria [144].

Žiemytė reported a chemically fueled Janus Pt-MSN nanomotor that can effectively penetrate the extracellular polymer and kill bacterial cells. Mesoporous silica NPs (MSN) serve as nanocontainers for the antibiotic vancomycin, with one side modified with Pt nanodendrites as a catalyst to decompose H_2O_2 into O_2, driving the movement of the nanomotor. The other side of MSN is externally modified with a gating system composed of a pH-sensitive inclusion complex between benzimidazole moieties and β-cyclodextrin

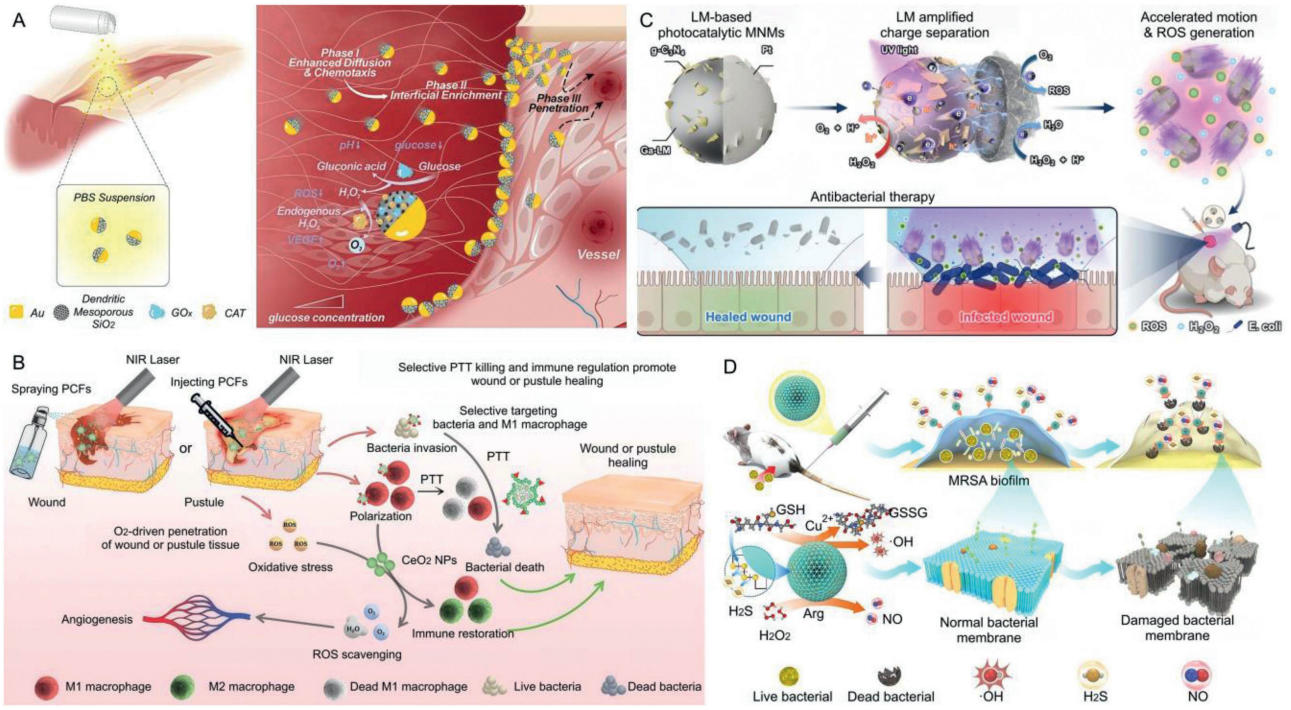


Fig. 11. Schematic diagrams of the nanomotors for wound-healing and antibacterial. (A) Schematic illustrations of the JNDMSNs for efficient treating diabetic wounds through hyperglycemia targeting and multifunctional wound microenvironment remodeling. Reprinted with permission [134]. Copyright 2025, Wiley-VCH. (B) Schematic diagram and mechanism of dual-targeting PCFs for deep anti-infection, anti-inflammation, and immunomodulation. Reprinted with permission [139]. Copyright 2025, Wiley-VCH. (C) Schematic of the LM-based photocatalytic MNMs for antibacterial therapy. Reprinted with permission [144]. Copyright 2025, American Chemical Society. (D) Schematic of a Dual-Gases-Driven Cu-tbDMSNs@Arg nanomotor used to treat mouse thigh infections. Reprinted with permission [145]. Copyright 2024, American Chemical Society.

(β-CD). β-CD is modified with ficin to disrupt the biofilm, synergistically and effectively killing bacteria with the antibiotic [146]. Zhai *et al.* designed a photothermally driven α-amylase-modified PDA pot-shaped nanomotor (APPNM). Under 808 nm NIR light irradiation, APPNM can efficiently propel in complex biological media and rapidly penetrate biofilms. The α-amylase immobilized on the surface of the nanomotor can destroy the dense structure of the biofilm by hydrolyzing polysaccharides in the biofilm, thus promoting the penetration of the nanomotor. The photothermal effect of PDA also improves the antibacterial efficiency. Due to its excellent biocompatibility, the designed nanomotor has great application potential in the field of biofilm-related infectious diseases [147].

Zheng *et al.* designed a nanomotor dual-driven by NO and H_2S gases (Fig. 11D). They incorporated Cu^{2+} and tetrasulfide into dendritic mesoporous silica NPs, then introduced the NO precursor L-arginine. In the biofilm microenvironment, highly expressed H_2O_2 oxidizes L-arginine to generate NO, while high-concentration GSH reacts with tetrasulfide to release H_2S. Cu^{2+} undergoes Fenton-like reactions to produce ROS. In a purulent myositis model infected with methicillin-resistant *Staphylococcus aureus* (MRSA), Cu-tbDMSNs@Arg showed significant tropism and accumulation at the infection site, eliminating bacteria. Released NO and H_2S reduced levels of pro-inflammatory factors TNF-α and IL-6, while increasing the anti-inflammatory factor IL-10 [145]. Bai *et al.* developed an asymmetric Janus nanomotor (J-CeM@Au) using mesoporous silica loaded with CeO_2 as the matrix, partially coated with AuNPs. Under NIR laser irradiation, AuNPs convert light energy into heat to drive nanomotor movement and produce bactericidal effects, further promoting biofilm penetration and clearance. CeO_2 nanozyme, with superoxide dismutase (SOD)-like and CAT-like activities, scavenges excessive ROS, alleviates inflammation, and induces macrophage polarization from M1 to M2 phenotypes. This nanomotor integrates the antibacterial properties of PTT, ROS scavenging, and immunomodulatory capabilities [148]. Through efficient ROS scavenging and autonomous movement, it promotes biofilm clearance, ensuring biocompatibility and reducing biotoxicity.

Bacterial microbes also cause food spoilage. Despite daily cleaning and disinfection, food processing machinery often harbors bacteria, some of which form biofilms [149]. Serena's group reported Janus nanomotors based on Pt and mesoporous silica, loaded with vanillin derivatives as antibacterial compounds. H_2O_2 triggers self-propelled movement, combining with vanillin's antibacterial activity to enhance elimination of multiple bacteria [150]. For drinking water pollution, He *et al.* designed a NO-driven nanomotor for large-scale water disinfection. Light-responsive NO donors generate NO under natural photocatalysis, powering the nanomotor to inhibit and eliminate pathogen biofilms [151].

The examples shown above illustrate that MNMs provide an innovative approach for antibacterial therapy, featuring "active targeting, synergistic bactericidal activity, and biofilm penetration". In particular, when combined with SDT, PTT and PDT, MNMs play a significant role in addressing challenging issues like drug-resistant bacterial treatment. For future development, biosecurity must still be taken into consideration to promote the translation of MNMs from laboratory research to clinical application.

3.5. Disease diagnosis

The treatment of diseases largely depends on the accuracy of early diagnosis. Current diagnostic methods include body fluid analysis tests, medical imaging, and biomarker monitoring. Compared with traditional nanomaterial probes, nanomotors have the ability of autonomous movement, faster moving speed, which enables them to interact with more substances to be detected in a short time, improving sensitivity. They also provide higher tissue penetration for diagnostic monitoring, efficiently capturing an-

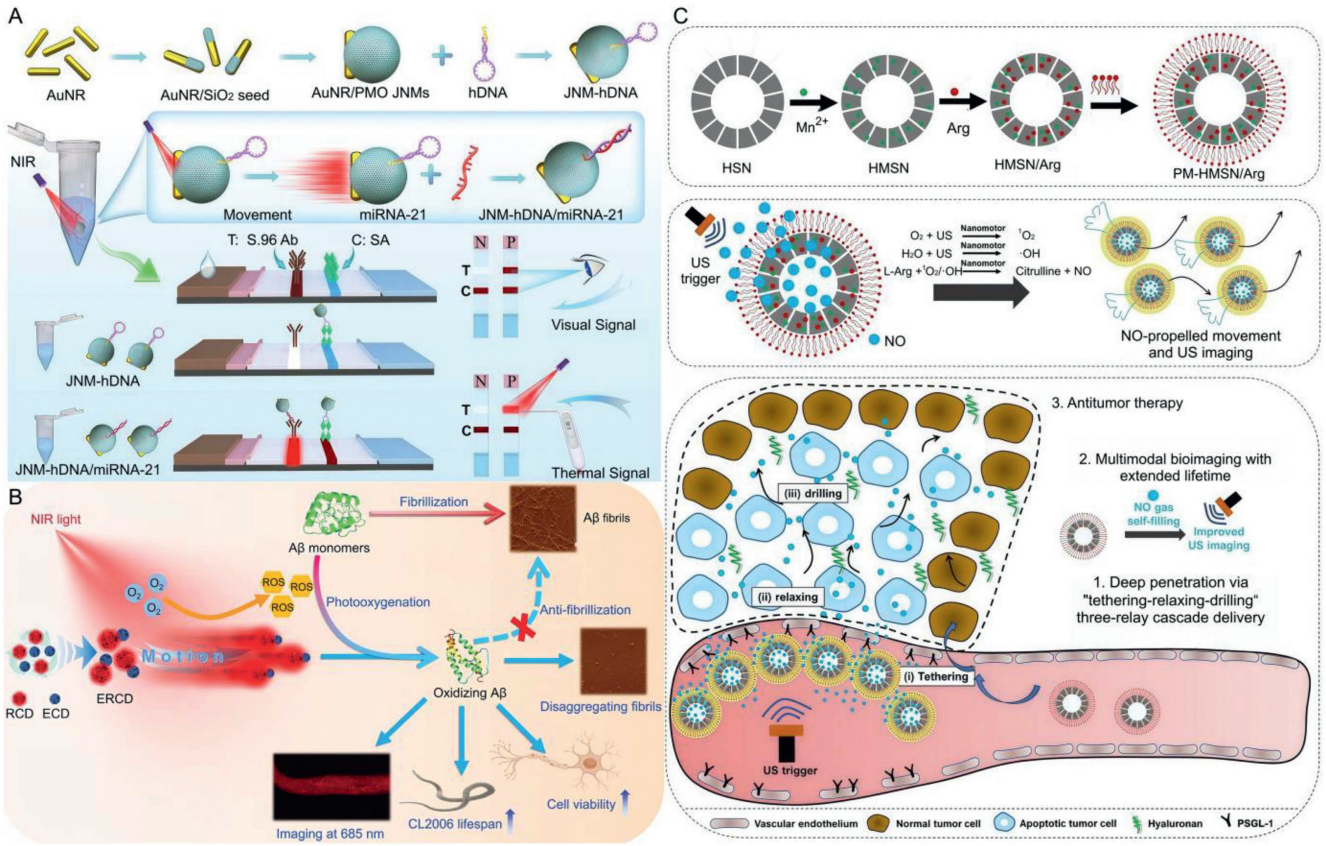


Fig. 12. Schematic diagrams of the nanomotors for disease diagnosis. (A) Schematic illustrations of the synthesis process of AuNR/PMO JNMs and principle of the AuNR/PMO JNM-assisted LFTS for rapid dual-modal and amplification-free detection of microRNA. Reprinted with permission [155]. Copyright 2023, American Chemical Society. (B) Schematic illustration of the multifunctionality light-driven nanomotor for the mitigation of Aβ-induced cytotoxicity and prolongation of AD nematode lifespan. Reprinted with permission [157]. Copyright 2024, Wiley-VCH. (C) Schematic of construction and motion mechanism of NO-driven nanomotor (PM-HMSN/Arg), which induces multimodal theranostics of cancer with deep penetration and extended lifetime [164]. Reprinted with permission. Copyright 2025, Wiley-VCH.

alytes in complex biological environments, thus offering a promising new direction for biological detection systems [152].

Dysregulated miRNA expression is associated with multiple diseases. Currently, lateral flow test strip (LFTS) technology has broad prospects due to its equipment-free operation, simplicity, and cost-effectiveness [153]. Dual-mode signal LFTS improves detection accuracy to a certain extent by using complementary signals as references, but it still needs to enhance the ability to capture miRNAs in complex body fluids or cells [154]. Based on this, Chen *et al.* designed a NIR light-driven Janus nanomotor with Au nanorods attached to mesoporous organosilica spheres, and deployed hDNA as a biorecognition element to construct a swimming AuNR/PMO JNM-hDNA probe for a dual-mode LFTS system for precise detection of miRNA-21 (Fig. 12A). AuNR/PMO JNM is expected to induce cell lysis to release miRNA-21, while acting as an active swimming biosensor to capture the released miRNA-21. Subsequently, the reacted solution is transferred to LFTS for analysis, generating dual-mode visual and thermal signals. The developed system was successfully applied to directly detect miRNA-21 in spiked serum samples and MDA-MB-231 cell lysates. Results show that AuNR/PMO JNM-assisted LFTS exhibits excellent performance in miRNA detection of complex biological samples, with low detection limits and short detection time [155]. Shen *et al.* also developed a self-driven TCPP-Fe@HMUiO@Au-ABEI nanoluminophore modified with CRISPR/Cas12a and 3D quadruplex DNA nanostructures, serving as a highly efficient biosensor for ultrasensitive detection of exomiR-155. Compared with previous detection methods, the exonuclease-driven nanomotor overcomes the drawback of low sensitivity of CRISPR/Cas12a, and TDNs can improve the trans-cleavage efficiency of Cas12a. Additionally, the large pore volume eliminates mass transfer limitations, the high specific surface area increases the concentration of surface catalytic active sites, and the confinement effect of mesopores positively impacts catalytic activity. Results indicate that this biosensor can accurately distinguish between healthy individuals and breast cancer patients. Nanomotors provide promising applications for constructing biological detection systems with high responsiveness and efficient signal amplification [156].

Lin *et al.* designed a light-driven nanomotor for detecting β-amyloid (Aβ), a biomarker of Alzheimer's disease (AD) (Fig. 12B). The light-driven nanomotor increases the contact chance between its surface and Aβ, enhancing the regulation of Aβ, which provides a new perspective for the development and application of multifunctional AD theranostic agents [157].

The detection of cancer-related markers is of great significance for the treatment of early-stage cancer patients [158]. Prostate cancer antigen 3 (PCA3) is an important disease biomarker of the prostate organ. When a small amount of prostate tissue undergoes early carcinogenesis, PCA3 is overexpressed in prostate cancer (PCa) tissues or metastatic foci [159]. Dou *et al.* synthesized hDNA probes labeled with Cy5 fluorophores and BHQ3 quenchers, and assembled hDNA probes with Fe_3O_4/Au NPs and Ure to form Janus nanomotor nanoprobes (JUNMs-hDNA). Immobilized Ure efficiently catalyzes the hydrolysis of urea to generate gas, driving the autonomous movement of nanoprobes. It identifies and captures the PCA3 sequence, activating the quenched fluorescence signal for precise and direct analysis. Additionally, the active self-propulsion of nanoprobes enables their efficient phagocytosis by

living cells to detect endogenous PCA3 in PCa cells. Therefore, JUNMs-hDNA nanoprobes provide a promising innovative technology for the direct and accurate detection of PCA3 in urine samples and living cells, offering a new approach for the early non-invasive clinical diagnosis of prostate cancer [160]. Deng *et al*. reported an ultrasensitive enzymatic nanomotor for detecting the tumor marker apurinic/apyrimidinic endonuclease 1 (APE1) released by cancer cell extracellular vesicles, which greatly improves the detection sensitivity [161]. Beltrán-Gastélum and co-workers reported an ultrasound-driven Au nanowire motor coated with graphene oxide on the surface, functionalized with fluorescein-labeled DNA aptamers (FAM-AIB1-apt) for qualitative detection of the overexpressed AIB1 oncoprotein in MCF-7 breast cancer cells. The movement of nanomotors under the ultrasound field promotes cell uptake, enabling faster binding of aptamers to target proteins and thus faster fluorescence recovery. Compared with static conditions, the propulsion behavior of aptamer-functionalized nanomotors significantly enhances the fluorescence intensity. This new aptamer-nanomotor-based strategy has great potential for further development of sensing methods for breast cancer diagnosis [162].

Dynamic imaging-guided precise diagnosis and treatment of cancer holds great potential in clinical applications, but it also faces the problem that the dense microenvironment of tumor tissues leads to insufficient penetration and accumulation of diagnostic and therapeutic nanomedicines, resulting in poor curative effects. Liu and collaborators designed a Janus-structured AIEgen nanomotor (M&P-NFT/R/DOX) to achieve deep tumor penetration and precise photodiagnosis and treatment. The nanomotor has both photothermal conversion and NIR-II fluorescence emission capabilities. Under laser irradiation, the heat generated by photothermal treatment forms a temperature gradient around the nanomotor, inducing thermophoretic force for propulsion. The heat can destroy tumor stromal cells and the ECM, reducing the resistance of tumor tissues and facilitating the effective propulsion of nanomotors in tumors, including cell uptake and intracellular distribution. NIR-II fluorescence is used for real-time monitoring of tumor diagnosis and intratumoral accumulation, synergizing with DOX for antitumor effects [163].

Xu *et al*. designed a NO-driven nanomotor for extended ultrasound imaging in cancer multimodal diagnosis and treatment (Fig. 12C). The NO nanogenerator produces NO to drive the motor movement, and the acoustically induced NO molecules diffuse into the tumor tissues, causing endothelial cell relaxation, allowing the nanomotor to penetrate deep into the tumor tissues through movement. NO is continuously generated *in situ* during ultrasound treatment. Due to the gas self-filling ability, the lifetime of the ultrasound imaging signal is greatly extended and its intensity is enhanced [164].

In the above examples, we have introduced the applications of MNMs in body fluid analysis and detection, medical imaging, and biomarker monitoring, which are involved in the diagnosis of diseases such as cancer and AD. The autonomous motion capability of MNMs enables them to efficiently capture analytes in complex biological environments, which enhances detection efficiency and thereby improves sensitivity and provides a promising new direction for biological detection systems. However, due to the complexity of body fluid samples, the capability of nanomotors may be affected by factors such as blood viscosity, leading to insufficient driving force. Additionally, nanomotors driven by light energy, ultrasound, or magnetic fields also require reliance on relevant equipment. This not only increases the application cost but also restricts the flexibility of its usage scenarios.

Nevertheless, in response to changes in the *in vivo* dynamic environment, nanomotors address the limitations of traditional NPs systems in overcoming biological barriers through active movement, flexible regulation, and precise control, promoting interactions between the motor and targets, reducing the time required for drug delivery and biosensing, and greatly improving treatment efficiency. endowing them with great development prospects in the field of biomedicine in the future.

4. Summary and outlook

In the past decade, significant efforts have been devoted to the research and application of MNMs. This review summarizes the design of MNMs with different driving mechanism. It particularly focuses on elaborating the latest advances of MNMs in the field of biomedicine, and explores and analyzes the application innovation.

Despite significant advancements in MNMs research, which has shown vast potential in biomedicine and promoted innovations in medical technology. MNMs still face interference from various factors when moving in complex *in vivo* environments, including ionic species, pH, temperature, blood flow viscosity, and immune clearance. NPs can induce the formation of endothelial cell gaps within a short exposure time. No published article has thus far addressed the induction of endothelial cell leakage by nanomotors. The ability of nanomotors to effectively penetrate biological barriers (such as the dense ECM in tumors and rigid bacterial biofilms) and reach the deep regions of diseased tissues is crucial for enhancing the efficiency of their biomedical applications. Ensuring consistent and stable driving performance of MNMs remains a challenge. Some nanomaterials such as catalytic metals, toxicity issues still exist. The residual of nanomaterials in organisms can cause damage to cells and tissues. Improving the biocompatibility and biosafety of MNMs is also an indispensable key link in enhancing their clinical application potential.

Based on this, the following suggestions can be adopted to improve the biosafety of nanomotors. (i) Selecting biocompatible nanomaterials for fabricating MNMs, such as FDA-approved biomaterials or cell membrane-coated MNMs, so as to improve the stability and circulation time of MNMs *in vivo*. (ii) It is essential to further study the interaction between MNMs and the immune system, in order to design motors that can avoid or regulate immune responses, thereby reducing inflammation and immune-mediated clearance. (iii) Designing smart-responsive functionalized MNMs modified with antibodies or targeting molecules can enhance their selectivity and improve biosafety. Controlling and regulating the movement of MNMs and drug release according to environmental changes and stimuli (such as external light, sound, magnetism) can reduce toxic side effects on non-target cells or tissues. (iv) Developing MNMs with self-destructive or self-clearing mechanisms can improve safety by ensuring timely clearance from the body after completing therapeutic tasks.

The suggestions are listed for achieving efficient and precise control over the movement of MNMs. (i) Multimodal-driven MNMs can avoid the drawback of insufficient sustained performance in single-mode driving and exhibit stronger motility. (ii) Integrating MNMs with medical imaging technologies such as photoacoustic imaging, ultrasound imaging, and magnetic resonance imaging, so as to achieve more precise control. (iii) As multifunctional therapeutic platforms, MNMs combined with other treatment modalities, including immunotherapy, CDT, and gene therapy, can better achieve diagnostic and therapeutic effects. (iv) Considering the issue of endothelial leakage, nanomotors with appropriate size, potential, and density should be prepared to enable their efficient enrichment and accumulation at the lesion site.

In conclusion, the future research should focus on the biosafety, driving efficiency, and controllability of MNMs, and collaborate across multidisciplinary fields such as materials science, medicine, engineering, and artificial intelligence to innovate, laying the foundation for the development of personalized and precision medicine to meet practical medical needs and promote clinical translation.

This review systematically sorts out the design concepts of MNMs and their applications in disease treatment, and deeply reveals their application potential in the field of precision medicine. The research not only provides theoretical support for the construction of micro-nano functional systems with low toxicity, high efficiency and environmental friendliness, but also strives to bring practically valuable reference insights to researchers in the fields of biology and medicine.

Declaration of competing interest

The authors declare that they have no known competing financial interests or personal relationships that could have appeared to influence the work reported in this paper.

CRediT authorship contribution statement

Xuan Hu: Writing – review & editing, Writing – original draft, Conceptualization. **Ziyan Shen:** Methodology, Conceptualization. **Shuang Chao:** Writing – review & editing, Conceptualization. **Yuxin Pei:** Validation, Supervision, Project administration. **Shoupeng Cao:** Writing – review & editing. **Zhichao Pei:** Writing – review & editing, Supervision, Project administration, Conceptualization.

Acknowledgments

This work was supported by the National Natural Science Foundation of China (Nos. 22571257, 22577103, 22301246, 52403198), and the Project of Science and Technology of Social Development in Shaanxi Province (Nos. 2023-YBSF-151, 2024SF-YBXM-294), and the Shaanxi Province Postdoctoral Science Foundation (No. 2023BSHEDZZ101). The authors thank the Teaching and Research Core Facility at College of Life Science, Life Science Research Core Services, and Crop Biology Innovation Center, Northwest A&F University for characterizations.

References

[1] B. Xu, B. Zhang, L. Wang, G. Huang, Y. Mei, Adv. Funct. Mater. 28 (2018) 1705872.
[2] Y. Hu, W. Liu, Y. Sun, Adv. Funct. Mater. 32 (2022) 2109181.
[3] Z. Shen, S. Chao, L. Wu, et al., Chem. Soc. Rev. 54 (2025) 8345–8405.
[4] Z. Liang, Y. Tu, F. Peng, Adv. Healthc. Mater. 10 (2021) 2100720.
[5] P. Liu, Y. Chang, X. Ren, et al., Green Chem. 25 (2023) 431–438.
[6] H. Huang, S. Yang, Y. Ying, et al., Adv. Mater. 36 (2024) 2305925.
[7] R.F. Ismagilov, A. Schwartz, N. Bowden, G.M. Whitesides, Angew. Chem. Int. Ed. 41 (2002) 652–654.
[8] T. Liu, L. Xie, C.A.H. Price, et al., Chem. Soc. Rev. 51 (2022) 10083–10119.
[9] L. Wang, M. Marciello, M. Estévez-Gay, et al., Angew. Chem. Int. Ed. 59 (2020) 21080–21087.
[10] S. Zhang, J. Li, X. Hu, et al., Chin. Chem. Lett. 36 (2025) 110314.
[11] H. Wang, G. Zhao, M. Pumera, J. Am. Chem. Soc. 136 (2014) 2719–2722.
[12] L. Gui, S. Wang, S. Miao, et al., Mater. Today Bio 33 (2025) 101950.
[13] X. Hu, Z. Shen, H. Hao, et al., J. Colloid Interface Sci. 694 (2025) 137688.
[14] T. Xu, F. Soto, W. Gao, et al., J. Am. Chem. Soc. 136 (2014) 8552–8555.
[15] L. Wang, Y. Zhang, C. Mao, X. Li, Adv. Sci. 11 (2024) 2405085.
[16] A. Mallick, S. Roy, Nanoscale 10 (2018) 12713–12722.
[17] W. Xu, H. Qin, H. Tian, et al., Appl. Mater. Today 27 (2022) 101482.
[18] K. Park, J. Controll. Rel. 305 (2019) 221–222.
[19] C.M. Cova, V. Ramos, A. Escudero, et al., Green Chem. 26 (2024) 11563–11575.
[20] M. Wan, H. Chen, Q. Wang, et al., Nat. Commun. 10 (2019) 966.
[21] J. Yu, Y. Li, A. Yan, et al., Adv. Sci. 10 (2023) 2301919.
[22] F. Lu, Y. Wang, D. Sun, et al., Green Chem. 27 (2025) 5400–5422.
[23] Y. Li, C. Shao, Z. Pei, Y. Pei, Green Chem. 27 (2025) 1871–1894.
[24] J. Yong, A.S. Mellick, J. Whitelock, J. Wang, K. Liang, Adv. Mater. 35 (2023) 2205746.
[25] H. Xu, M. Medina-Sánchez, M.F. Maitz, C. Werner, O.G. Schmidt, ACS Nano 14 (2020) 2982–2993.
[26] F. Zhang, Z. Li, Y. Duan, et al., Sci. Rob. 7 (2022) eabo4160.
[27] J. Wu, L. Liu, B. Chen, et al., Appl. Mater. Today 25 (2021) 101197.
[28] H. Xu, M. Medina-Sánchez, V. Magdanz, et al., ACS Nano 12 (2018) 327–337.
[29] J. Chen, Y. Qiao, B. Tang, et al., Theranostics 7 (2017) 2250–2260.
[30] W. Chen, Y. Wang, M. Qin, et al., ACS Nano 12 (2018) 5995–6005.
[31] M. Zhang, H. Nie, G. Jiang, et al., Nano Today 63 (2025) 102752.
[32] C.H. Luo, C.T. Huang, C.H. Su, C.S. Yeh, Nano Lett. 16 (2016) 3493–3499.
[33] M. Wu, W. Wu, Y. Duan, et al., Chem. Mater. 31 (2019) 7212–7220.
[34] M.M. Stanton, J. Simmchen, X. Ma, A. Miguel-López, S. Sánchez, Adv. Mater. Interfaces 3 (2016) 1500505.
[35] F. Zhang, Z. Li, Y. Duan, et al., Sci. Adv. 8 (2022) eade6455.
[36] Z. Lin, C. Gao, D. Wang, Q. He, Angew. Chem. Int. Ed. 60 (2021) 8750–8754.
[37] Z. Wang, Y. Yan, C. Li, et al., ACS Nano 16 (2022) 9019–9030.
[38] S. Liang, J. Xing, Z. Zhang, et al., Small 21 (2025) 2500207.
[39] H. Zhou, Q. Liu, M. Chen, et al., ACS Sens. 10 (2025) 1155–1165.
[40] T. Bao, N. Li, H. Chen, et al., ACS Appl. Mater. Interfaces 15 (2023) 32762–32771.
[41] Z. Xiao, Y. Li, T. Chen, et al., Chem. Eng. J. 496 (2024) 154205.
[42] W. Wang, Z. Zhao, Z. Zhang, et al., J. Controll. Rel. 377 (2025) 648–660.
[43] L. Liu, Q. Li, L. Chen, et al., Chem. Sci. 13 (2022) 12840–12850.
[44] H. Chi, W. Wu, H. Bao, Y. Wu, N. Hu, Adv. Healthc. Mater. 14 (2025) 2404303.
[45] B. Wu, J. Fu, Y. Zhou, et al., Acta Pharm. Sin. B 10 (2020) 2198–2211.
[46] K. Zhang, Y. Long, S. Li, Y. Zhao, H. Han, Nano Today 55 (2024) 102171.
[47] H. Choi, S.H. Cho, S.K. Hahn, ACS Nano 14 (2020) 6683–6692.
[48] Z. Liu, S. Liu, X. Zhao, et al., Int. J. Biol. Macromol. 240 (2023) 124486.
[49] Z. Zhao, X. Shan, H. Zhang, et al., J. Controll. Rel. 362 (2023) 151–169.
[50] K.M. Miranda, L.A. Ridnour, C.L. McGinity, D. Bhattacharyya, D.A. Wink, Inorg. Chem. 60 (2021) 15941–15947.
[51] H. Chen, T. Li, Z. Liu, et al., Nat. Commun. 14 (2023) 941.
[52] M. Wan, Z. Liu, T. Li, et al., Angew. Chem. Int. Ed. 60 (2021) 16139–16148.
[53] Z. Wu, M. Zhou, X. Tang, et al., ACS Nano 16 (2022) 3808–3820.
[54] D. Wu, W. Si, M. Wang, et al., Nitric Oxide 50 (2015) 38–45.
[55] Z. Zhao, L. Chen, C. Yang, et al., Bioact. Mater. 31 (2024) 578–589.
[56] N. Li, C. Huang, J. Zhang, et al., ACS Nano 17 (2023) 12573–12593.
[57] W. Yu, R. Lin, X. He, et al., Acta Pharm. Sin. B 11 (2021) 2924–2936.
[58] L. Liu, X. Li, Y. Chen, et al., Nat. Commun. 16 (2025) 2339.
[59] H. Choi, S.h. Jeong, C. Simó, et al., Nat. Commun. 15 (2024) 9934.
[60] Y. Pan, X. Ma, Y. Wu, et al., Colloids Surf. A 684 (2024) 133070.
[61] W. Ban, J. Qu, L. Cai, et al., Appl. Mater. Today 34 (2023) 101916.
[62] L. Wang, Y. Huang, H. Xu, et al., Mater. Today Chem. 26 (2022) 101059.
[63] Z. Zhang, H. Zhong, Y. Zhou, et al., Nano Today 45 (2022) 101542.
[64] M.A. Ramos-Docampo, M. Fernández-Medina, E. Taipaleenmäki, et al., ACS Nano 13 (2019) 12192–12205.
[65] J. Zhang, Z. Chen, R.K. Kankala, S.B. Wang, A.Z. Chen, Int. J. Pharm. 596 (2021) 120275.
[66] M. Mathesh, J. Sun, D.A. Wilson, J. Mater. Chem. B 8 (2020) 7319–7334.
[67] M. Hosseini, F. Babayekhorasani, Z. Guo, et al., J. Colloid Interface Sci. 628 (2022) 435–445.
[68] X. Liu, Y. Wang, L. Wang, W. Chen, X. Ma, Small 20 (2024) 2305800.
[69] A.C. Hortelao, C. Simó, M. Guix, et al., Sci. Rob. 6 (2021) eabd2823.
[70] Y. Liu, R. Terracciano, J. Scheerstra, et al., Angew. Chem. Int. Ed. 64 (2025) e202505717.
[71] L. Wang, A.C. Hortelão, X. Huang, S. Sánchez, Angew. Chem. Int. Ed. 58 (2019) 7992–7996.
[72] J. Wu, S. Ma, M. Li, et al., ACS Appl. Mater. Interfaces 13 (2021) 31514–31526.
[73] K. Mayolo-Deloisa, M. González-González, M. Rito-Palomares, Front. Bioeng. Biotechnol. 8 (2020) 222.
[74] V. Bhandari, C. Hoey, L.Y. Liu, et al., Nat. Genet. 51 (2019) 308–318.
[75] Q. Chen, L. Si, P. Qin, et al., J. Mater. Chem. B 13 (2025) 8897–8907.
[76] J. Wang, X. Liu, Y. Qi, et al., Chem. Eng. J. 416 (2021) 129091.
[77] J. Feng, S.P. Yang, Y.Q. Shao, et al., Adv. Healthc. Mater. 12 (2023) 2301645.
[78] Y. Zhang, Y. Xing, H. Zhou, et al., Acta Biomater. 190 (2024) 463–475.
[79] Y. Wang, W. Chen, Z. Wang, et al., Angew. Chem. Int. Ed. 62 (2023) e202212866.
[80] K. Ma, J. Dong, Z. Chen, et al., Chem. Eng. J. 512 (2025) 162107.
[81] Z.H. Wang, X. Zeng, S. Zhang, et al., ACS Nano 19 (2025) 17228–17246.
[82] X. Fan, H. Chen, Y. Li, et al., ACS Nano 19 (2025) 6454–6467.
[83] B. Qiu, L. Xie, J. Zeng, et al., Adv. Funct. Mater. 31 (2021) 2010694.
[84] J. Meng, W. Wei, S. Xie, et al., Chem. Eng. J. 501 (2024) 157763.
[85] J. Zhang, K. Zhang, Y. Hao, et al., J. Colloid Interface Sci. 633 (2023) 679–690.
[86] Y. Xing, J. Xiu, M. Zhou, et al., ACS Nano 17 (2023) 6789–6799.
[87] A. Indini, D. Massi, M. Pirro, et al., Semin. Cancer Biol. 86 (2022) 477–490.
[88] Y. Deng, J. Zheng, J. Li, et al., Theranostics 15 (2025) 3474–3489.
[89] Z. Yuan, J. Wu, Y. Xiao, et al., Adv. Funct. Mater. 33 (2023) 2302908.
[90] L. Liu, S. Li, K. Yang, et al., Nano Lett. 23 (2023) 3929–3938.
[91] W. Wang, L.A. Castro, M. Hoyos, T.E. Mallouk, ACS Nano 6 (2012) 6122–6132.
[92] Y. Cao, S. Liu, Y. Ma, et al., Small 18 (2022) 2203466.
[93] M. Hansen-Bruhn, B.E.-F. de Ávila, M. Beltrán-Gastélum, et al., Angew. Chem. Int. Ed. 57 (2018) 2657–2661.
[94] F. Zhang, J. Zhuang, B. Esteban Fernández de Ávila, et al., ACS Nano 13 (2019) 11996–12005.
[95] T. Chen, J. Yang, H. Zhao, et al., J. Mater. Chem. B 12 (2024) 667–677.
[96] X. Yu, X. Li, Q. Chen, et al., Adv. Sci. 11 (2024) 2305546.
[97] W. Gao, B.E.F. de Ávila, L. Zhang, J. Wang, Adv. Drug Deliv. Rev. 125 (2018) 94–101.
[98] T. Zhou, K. Zhu, Z. Yang, et al., Small 20 (2024) 2311207.
[99] Z. An, E. Lin, Z. Wu, Y. Kang, J. Mater. Chem. B 13 (2025) 1296–1301.
[100] Z. Liu, T. Xu, M. Wang, C. Mao, B. Chi, J. Mater. Chem. B 8 (2020) 11055–11062.
[101] X. Wang, X. Dai, Y. Chen, Small 19 (2023) 2301693.
[102] S. Zhang, L. Wu, W. Shi, et al., Adv. Funct. Mater. 33 (2023) 2302360.
[103] J. Meng, P. Zhang, Q. Liu, et al., Acta Biomater. 162 (2023) 20–31.
[104] J. Meng, K. Wei, S. Xie, et al., J. Controll. Rel. 357 (2023) 342–355.

[105] X. Zhang, Y. Lyu, J. Li, et al., Adv. Funct. Mater. 34 (2024) 2406059.
[106] Q. Li, L. Liu, H. Huo, et al., ACS Nano 16 (2022) 7947–7960.
[107] E. Ma, K. Wang, Y. Gou, W. Luo, H. Wang, Small 21 (2025) 2404703.
[108] K. Lv, M. Hou, Y. Kou, et al., ACS Nano 18 (2024) 13910–13923.
[109] X. Zhang, C. Liu, J. Li, et al., J. Colloid Interface Sci. 657 (2024) 799–810.
[110] Z. Hu, H. Tan, Y. Ye, et al., Adv. Mater. 36 (2024) 2412227.
[111] X. Wang, H. Ma, Y. Guo, J. Zhang, X. Han, Chem. Eng. J. 490 (2024) 151777.
[112] A.M. Florea, D. Büsselberg, Cancers 3 (2011) 1351–1371.
[113] N.A.G.d. Santos, R.S. Ferreira, A.C.d. Santos, Food Chem. Toxicol. 136 (2020) 111079.
[114] L. Xu, K. Zhang, X. Ma, et al., J. Nanobiotechnol. 20 (2022) 429.
[115] J. Ye, Q. Fu, L. Liu, et al., Sci. China Chem. 64 (2021) 2218–2229.
[116] M. Weller, P.Y. Wen, S.M. Chang, et al., Nat. Rev. Dis. Primers 10 (2024) 33.
[117] G.C. Terstappen, A.H. Meyer, R.D. Bell, W. Zhang, Nat. Rev. Drug Discov. 20 (2021) 362–383.
[118] J. Ye, Y. Fan, Y. Kang, et al., Adv. Funct. Mater. 35 (2025) 2416265.
[119] T. Li, L. Chen, Y. Xue, et al., Sci. China Chem. 67 (2024) 1277–1288.
[120] W. Zhang, Y. Xiang, Q. Guo, et al., Acta Biomater. 191 (2025) 352–368.
[121] L. Galluzzi, G. Kroemer, Nat. Immunol. 23 (2022) 1300–1302.
[122] Z. Liu, X. Luan, Q. Lu, et al., Nat. Commun. 16 (2025) 4708.
[123] P.L. Lutsey, N.A. Zakai, Nat. Rev. Cardiol. 20 (2023) 248–262.
[124] M. Juenet, R. Aid-Launais, B. Li, et al., Biomaterials 156 (2018) 204–216.
[125] M. Wan, Q. Wang, R. Wang, et al., Sci. Adv. 6 (2020) eaaz9014.
[126] H. Zhang, K. Cao, C. Wang, Y. Tian, L. Hou, Chem. Eng. J. 498 (2024) 155054.
[127] D. Fang, T. Li, Z. Wu, et al., J. Mater. Chem. B 9 (2021) 8659–8666.
[128] Y. Su, L. Huang, G. Xu, et al., Adv. Healthc. Mater. 14 (2025) 2404960.
[129] R. Ruan, S. Chen, J. Su, et al., Adv. Healthc. Mater. 13 (2024) 2302591.
[130] F. Soto, J. Wang, R. Ahmed, U. Demirci, Adv. Sci. 7 (2020) 2002203.
[131] Y. Xia, Z. Chen, X. Zhang, P. Yang, Z. Wang, Adv. Mater. 37 (2025) 2418590.
[132] M.G. Monaghan, R. Borah, C. Thomsen, S. Browne, Adv. Drug Deliv. Rev 203 (2023) 115120.
[133] J. Hu, L. Xu, J. Cao, et al., J. Colloid Interface Sci. 679 (2025) 747–759.
[134] J. Lin, C. Lian, L. Xu, et al., Adv. Funct. Mater. 35 (2025) 2417146.
[135] L. Kong, Z. Wu, H. Zhao, et al., ACS Appl. Mater. Interfaces 10 (2018) 30103–30114.
[136] S. Xie, K. Huang, J. Peng, et al., Adv. Healthc. Mater. 11 (2022) 2201323.
[137] C.E. Heim, M.E. Bosch, K.J. Yamada, et al., Nat. Microbiol. 5 (2020) 1271–1284.
[138] J. Zheng, Y. Deng, S. Zhao, et al., Chem. Eng. J. 481 (2024) 148790.
[139] W. Wang, Y. Gao, Y. Lin, et al., Adv. Funct. Mater. 35 (2025) 2416684.
[140] A.E. Clatworthy, E. Pierson, D.T. Hung, Nat. Chem. Biol. 3 (2007) 541–548.
[141] S.B. Levy, B. Marshall, Nat. Med. 10 (2004) S122–S129.
[142] M. Kiristi, V.V. Singh, B. Esteban-Fernández de Ávila, et al., ACS Nano 9 (2015) 9252–9259.
[143] X. Li, H. Shang, Y. Xiong, et al., Chem. Eng. J. 505 (2025) 159367.
[144] Z. Guo, D. Jin, H. Li, et al., ACS Nano 19 (2025) 20037–20050.
[145] J. Zheng, H. Liu, Y. Deng, et al., ACS Mater. Lett. 6 (2024) 5128–5137.
[146] M. Žiemytė, A. Escudero, P. Díez, et al., Chem. Mater. 35 (2023) 4412–4426.
[147] X. Zhai, Y. Liu, X. Hao, et al., Adv. Healthc. Mater. 14 (2025) 2403033.
[148] X. Bai, W. Peng, Y. Tang, et al., Bioact. Mater. 41 (2024) 271–292.
[149] M. Sadekuzzaman, S. Yang, M.F.R. Mizan, S.D. Ha, Compr. Rev. Food Sci. Food Saf. 14 (2015) 491–509.
[150] S. Medaglia, A. Escudero, Á. Morellá-Aucejo, et al., Food Res. Int. 212 (2025) 116510.
[151] Z. He, Y. Li, L. Yang, et al., J. Colloid Interface Sci. 665 (2024) 634–642.
[152] A. Rastmanesh, M. Tavakkoli Yaraki, J. Wu, et al., Mol. Syst. Des. Eng. 6 (2021) 566–593.
[153] C. Parolo, A. Sena-Torralba, J.F. Bergua, et al., Nat. Protoc. 15 (2020) 3788–3816.
[154] C.C. Pritchard, H.H. Cheng, M. Tewari, Nat. Rev. Genet. 13 (2012) 358–369.
[155] M. Chen, E. Ma, Y. Xing, et al., ACS Sens. 8 (2023) 757–766.
[156] B. Shen, L. Li, C. Liu, et al., Anal. Chem. 95 (2023) 4486–4495.
[157] X. Lin, X. Dong, Y. Sun, Small 20 (2024) 2407154.
[158] C.S. McNevin, A.M. Baird, R. McDermott, S.P. Finn, Diagnostics 11 (2021) 345.
[159] Y. Mitobe, K.i. Takayama, K. Horie-Inoue, S. Inoue, Cancer Lett. 418 (2018) 159–166.
[160] P. Dou, Q. Liu, M. Chen, et al., Sens. Actuat. B 426 (2025) 137051.
[161] J. Deng, S. Zhao, K. Xie, et al., Angew. Chem. Int. Ed. 64 (2025) e202417165.
[162] M. Beltrán-Gastélum, B. Esteban-Fernández de Ávila, H. Gong, et al., ChemPhysChem 20 (2019) 3177–3180.
[163] M. Liu, H. Tan, B.B. Chen, et al., ACS Nano 19 (2025) 21068–21082.
[164] X. Xu, J. Cao, Y. Mu, et al., Adv. Sci. 12 (2025) e16709.